

# Cross-Laboratory Experimental Study of Non-Noble-Metal Electrocatalysts for the Oxygen Reduction Reaction

Frédéric Jaouen,<sup>\*,†</sup> Juan Herranz,<sup>†</sup> Michel Lefèvre,<sup>†</sup> Jean-Pol Dodelet,<sup>†</sup> Ulrike I. Kramm,<sup>‡</sup> Iris Herrmann,<sup>‡</sup> Peter Bogdanoff,<sup>‡</sup> Jun Maruyama,<sup>§</sup> Toru Nagaoka,<sup>||</sup> Arnd Garsuch,<sup>⊥</sup> Jeff R. Dahn,<sup>⊥</sup> Tim Olson,<sup>#</sup> Svitlana Pylypenko,<sup>#</sup> Plamen Atanassov,<sup>#</sup> and Eugene A. Ustinov<sup>∇</sup>

Institut National de la Recherche Scientifique, Énergie, Matériaux & Télécommunications, 1650 Bd Lionel Boulet, Varennes, Québec J3X 1S2, Canada, Helmholtz-Zentrum Berlin GmbH, Lise-Meitner-Campus, Glienicker Strasse 100, 14 109 Berlin, Germany, Environmental Technology Research Division and Processing Technology Research Division, Osaka Municipal Technical Research Institute, 1-6-50 Morinomiya, Joto-Ku, Osaka 536-8553, Japan, Department of Physics and Atmospheric Science, Dalhousie University, Halifax, Nova Scotia B3H 3J5, Canada, Chemical & Nuclear Engineering Department, University of New Mexico, Albuquerque, New Mexico 87131, and Ioffe Physical Technical Institute, Polytechnicheskaya 26, St. Petersburg 194021, Russian Federation

**ABSTRACT** Nine non-noble-metal catalysts (NNMCs) from five different laboratories were investigated for the catalysis of O<sub>2</sub> electroreduction in an acidic medium. The catalyst precursors were synthesized by wet impregnation, planetary ball milling, a foaming-agent technique, or a templating method. All catalyst precursors were subjected to one or more heat treatments at 700–1050 °C in an inert or reactive atmosphere. These catalysts underwent an identical set of electrochemical characterizations, including rotating-disk-electrode and polymer–electrolyte membrane fuel cell (PEMFC) tests and voltammetry under N<sub>2</sub>. Ex situ characterization was comprised of X-ray photoelectron spectroscopy, neutron activation analysis, scanning electron microscopy, and N<sub>2</sub> adsorption and its analysis with an advanced model for carbonaceous powders. In PEMFC, several NNMCs display mass activities of 10–20 A g<sup>-1</sup> at 0.8 V versus a reversible hydrogen electrode, and one shows 80 A g<sup>-1</sup>. The latter value corresponds to a volumetric activity of 19 A cm<sup>-3</sup> under reference conditions and represents one-seventh of the target defined by the U.S. Department of Energy for 2010 (130 A cm<sup>-3</sup>). The activity of all NNMCs is mainly governed by the microporous surface area, and active sites seem to be hosted in pore sizes of 5–15 Å. The nitrogen and metal (iron or cobalt) seem to be present in sufficient amounts in the NNMCs and do not limit activity. The paper discusses probable directions for synthesizing more active NNMCs. This could be achieved through multiple pyrolysis steps, ball-milling steps, and control of the powder morphology by the addition of foaming agents and/or sulfur.

**KEYWORDS:** non-platinum group metal • catalyst • oxygen electroreduction • fuel cell • polymer electrolyte

## I. INTRODUCTION

Since the advent in the 1960s of perfluorinated polymers with proton conductivity of  $\sim 10 \text{ S m}^{-1}$  (1), the research and development in low-temperature fuel cells (<100 °C) has progressively become dominated by polymer–electrolyte membrane fuel cells (PEMFCs). Reinforced 20–30- $\mu\text{m}$ -thick polymer membranes with resistances as low as 20–30 m $\Omega \text{ cm}^2$  are now available. This great advancement in acidic PEMs has, however, placed the burden on the electrocatalysis side. While hydrogen oxida-

tion is fast (2), the oxygen reduction reaction (ORR) is sluggish at any pH. Therefore, the ORR requires the best possible catalysts. However, while at high pH ORR electrocatalysts can be chosen from a large repertoire (Pt, Pd, Ag, Au, Ni–Co spinel oxides, manganese oxides, and iron or cobalt phthalocyanines or porphyrins) (3–12) the acidic character of PEM precludes the use of most of these catalysts for reasons of either poor stability or activity. Today, Pt is the only viable catalyst for ORR in PEMFC, but still the cathode is the least efficient component. For reasons of cost, the meaningful ORR activity of a Pt catalyst is the current obtained per Pt mass at a fixed cathode potential. This ratio is called the mass activity.

The experimental conditions prevailing for reporting the Pt mass activity for the ORR in a PEMFC are a cell voltage of 0.9 V, O<sub>2</sub> and H<sub>2</sub> pressures of 1 bar, 100% relative humidity (RH), and a temperature of 80 °C (13, 14). The Pt mass activity has been dramatically improved by tailoring Pt in particles of 2–5 nm supported on carbon (Pt/C), alloying Pt with Ti, V, Cr, Mn, Fe, Co, or Ni (13, 15–20), optimizing the catalyst–polymer electrolyte contact in porous cathodes (21–23), or depositing a Pt monolayer on Au or Pd nano-

\* Phone: +1 929 8176. Fax: +1 929 8102. E-mail: jaouen@emt.inrs.ca.  
Received for review March 31, 2009 and accepted July 8, 2009

<sup>†</sup> Institut National de la Recherche Scientifique, Énergie, Matériaux & Télécommunications.

<sup>‡</sup> Helmholtz-Zentrum Berlin GmbH.

<sup>§</sup> Environmental Technology Research Division, Osaka Municipal Technical Research Institute.

<sup>||</sup> Processing Technology Research Division, Osaka Municipal Technical Research Institute.

<sup>⊥</sup> Dalhousie University.

<sup>#</sup> University of New Mexico.

<sup>∇</sup> Ioffe Physical Technical Institute.

DOI: 10.1021/am900219g

© 2009 American Chemical Society

particles (24–26). Thus, the Pt loadings could be reduced from  $28 \text{ mg cm}^{-2}$  with unsupported Pt (27) to  $0.8 \text{ mg cm}^{-2}$  today (0.4 per electrode) (13). The targeted Pt loading for automotive application is  $0.1 \text{ mg cm}^{-2}$  per electrode in 2015 (14). While a negligible performance decay occurs when the anode Pt loading is reduced from 0.4 to  $0.1 \text{ mg cm}^{-2}$  (28), an equal reduction at the cathode without adverse effects on the performance requires that the mass activity of Pt catalysts be increased by 4-fold.

Paradoxically, recent improvements in the PEMFC performance and its probable emergence as a consumer good have revived the problems of Pt availability and cost, which are the fundamental incentives to search for non-noble metal catalysts (NNMCs) (29). Even if the U.S. Department of Energy (DOE) target for year 2015 of  $0.2 \text{ g of Pt kW}^{-1}$  is achieved, a scenario of an all-PEMFC car production of, say, 100 million cars a year (in 2007, 73 million cars and trucks were produced worldwide (30)) with engines rated at 50 kW would require 1000 tons of Pt a year. In 2007, the Pt world production amounted to only 204 tons, 60% of it being installed in catalytic converters for exhaust cleaning of internal combustion engines (ICEs) (31). While an average-size gasoline ICE vehicle requires only 1 g of Pt, 10 g is expected for a PEMFC vehicle. On the other hand, *diesel* ICE vehicles contain on average, in Europe, 5 g of Pt (in 2007, 59 tons of Pt (31) were used to produce  $\sim 11$  million European diesel vehicles (30)). Increased Pt demand and stagnating Pt production triggered the Pt price increase from 600 to 2100 \$/oz from 2003 to mid-2008 (32). In the long term, however, there could be enough Pt on earth to produce 3 billion PEMFC cars over the next 100–150 years at the actual Pt mining rate (33, 34). However, is it sound to deplete the reserves of that, in many applications, irreplaceable metal? It is also questionable whether a recycling rate of  $>95\%$  of the Pt to be contained in PEMFC is feasible. This is necessary for a sustainable worldwide PEMFC car fleet.

A renewed interest in NNMCs for the ORR occurred a few years ago, and targets of activity were defined (14). The practical activity for NNMCs is defined on a different ground than that for Pt-on-C catalysts (Pt/C). Because NNMCs have a negligible cost against other PEMFC components, the concept of mass activity, so important for Pt for reasons of cost, could at first sight appear to be out of place for NNMCs. One might consider increasing the loading of poorly active NNMCs by a factor of 50–100 versus the actual Pt loading in order to match the performance of a Pt-based cathode. Unfortunately,  $\text{O}_2$  diffusion and proton and electron conductivity across the porous cathode are impervious to the possible cost advantage of NNMCs. The maximum NNMC loading that can be efficiently utilized under a practical current density of  $>1 \text{ A cm}^{-2}$  is restricted by the mass- and charge-transport characteristics of the cathode. Today's Pt-based cathodes ( $0.4 \text{ mg of Pt cm}^{-2}$ ; 45–50 wt % Pt on carbon) are about  $10 \mu\text{m}$  thick. In a first attempt to define the target of activity for NNMCs, the maximum thickness envisaged for an efficient NNMC cathode was set to  $100 \mu\text{m}$  (13). It follows that, in order for an NNMC cathode to equal

the kinetic performance of today's Pt-based cathodes, an NNMC should display no less than one-tenth of the ORR activity of Pt/C, with the activity being defined by the current *per volume of porous cathode*. This ratio is called the volumetric activity. The potential chosen to report the NNMC activity was downscaled to 0.8 V (13) because the activity was too low to be measurable at 0.9 V. Under reference conditions ( $\text{O}_2$  and  $\text{H}_2$  pressures of 1 bar; 100% RH;  $80^\circ\text{C}$ ), the U.S. DOE targets for the NNMC activity were set at 130 (year 2010) and  $300 \text{ A cm}^{-3}$  (year 2015) (14). The 2010 target represents one-tenth of the volumetric activity at 0.8 V of a Pt/C cathode in year 2005:  $1300 \text{ A cm}^{-3}$  (Supporting Information, section A).

NNMCs for the ORR in an acidic medium can be divided in (i) inorganic catalysts and (ii) molecular or molecular-derived catalysts. Only a few inorganic structures with non-noble metals catalyze the ORR in an acidic medium, and their activities have been, up to now, quite poor. Chalcogenides (35–38), nitrides (39, 40), and oxides (41, 42) have been investigated. The second class of NNMCs, which is the focus of this paper, was introduced when Jasinski discovered that cobalt phthalocyanine catalyzes the ORR in an alkaline medium (3). Later, the same molecule as well as other metal- $\text{N}_4$  chelates was found to catalyze the ORR in an acidic medium as well (43). Since then, metal- $\text{N}_4$  chelates have served as biomimetic analogues of cytochromes that are key molecules for the respiratory chain (44–49). An important step was the discovery that a high-temperature treatment ( $400\text{--}1000^\circ\text{C}$ ) of metal- $\text{N}_4$  chelates in an inert gas increased the stability and activity (50–57). Because these molecules decompose at such temperatures, the nature of the active sites following the heat treatment has ever since been a subject of controversy (52–56, 58–60). A second important step came with the high-temperature synthesis of an NNMC free of metal- $\text{N}_4$  chelate. Polyacrylonitrile mixed with  $\text{Co}^{\text{II}}$  or  $\text{Fe}^{\text{II}}$  salt was heat treated at  $800^\circ\text{C}$  under argon (61). This work concluded that the high-temperature synthesis of an NNMC requires the simultaneous presence of a transition metal, N, and C. In that work, the N and C sources were still joint (polyacrylonitrile). In a third step, it was shown that all three sources of a transition metal, N, and C could be separately introduced in the oven. Gaseous sources for N were introduced in 1998–1999 in the form of  $\text{CH}_3\text{CN}$  or  $\text{NH}_3$  (62, 63).

Since 1990, many groups have synthesized NNMCs using a single or several heat-treatment steps; metal- $\text{N}_4$  chelates or metal salts as a metal source; metal- $\text{N}_4$  chelates, molecules, polymers, or  $\text{NH}_3$  or  $\text{CH}_3\text{CN}$  gases as a N source; metal- $\text{N}_4$  chelates, molecules, polymers, or carbon powders as a C source (64–98). The heat treatment of unsupported molecules may result in a low-porosity catalyst. To increase the porosity, a foaming agent can be added. This technique has been applied on iron(III) chloride 5,10,15,20-tetrakis(4-methoxyphenyl)porphyrin (FeClTMPP) and cobalt(II) 5,10,15,20-tetrakis(4-methoxyphenyl)porphyrin (CoTMPP) with iron oxalate as the foaming agent (71, 73, 84, 91).

The present spotlight aims to answer two important questions:

What is the present activity for the ORR of NNMCs obtained from a heat treatment and how does it compare to U.S. DOE targets?

Does one physicochemical characteristic of the NNMC or a combination of such characteristics explain their ORR activity, regardless of the sources of metal, N, and C used for their synthesis?

NNMCs obtained through a heat treatment were synthesized according to different schemes (diverse metal, N, and C precursors) at different laboratories and shipped to the Institut National de la Recherche Scientifique (INRS) between September 2007 and May 2008. Rotating-disk-electrode (RDE) and PEMFC tests were performed. For each catalyst, PEMFC tests with different ink recipes (Nafion/catalyst ratio) or NNMC loadings were run. Ex situ characterization was comprised of X-ray photoelectron spectroscopy (XPS), neutron activation analysis (NAA), N<sub>2</sub> adsorption and its analysis with an advanced model for carbonaceous powders, and scanning electron microscopy (SEM).

All reported experimental results are based on new measurements, not on previously published measurements, except for some data points in Figures 9–11 (see the figure captions).

## II. EXPERIMENTAL METHODS

**II.1. Catalyst Synthesis.** For space reasons, the fully detailed synthesis of all catalysts is given in the Supporting Information, section B. For all catalysts, at least one heat-treatment step is involved and there is at least one source of N, C, and Fe (or Co). The acronyms of the catalysts are UK63, UK65, CHb200900, CoTMPP700, GAdFeCu, DAL900A, DAL900C, FC280, and M786. The catalysts can be classified according to four synthesis approaches:

Approach i uses a metal–N<sub>4</sub> chelate as the exclusive or main precursor for metal, N, and C. Pyrolysis is made in an inert gas. In two instances (UK63 and UK65), iron oxalate is added to obtain high surface areas. Catalysts made according to approach i are UK63, UK65, CHb200900, and CoTMPP700.

The second approach (ii) uses a metal salt as the exclusive metal precursor and a N-containing molecule as the exclusive N source. No preexisting C support is used. Pyrolysis is carried out under an inert atmosphere. Catalysts investigated in the present paper that correspond to approach ii are GAdFeCu and DAL900A.

A third approach (iii) consists of performing a second heat treatment under a reactive atmosphere to catalysts that have undergone a first heat treatment under an inert atmosphere (approaches i and ii). The reactive atmosphere could be oxidative (O<sub>2</sub> and CO<sub>2</sub>) or reductive (NH<sub>3</sub> and N<sub>2</sub>/H<sub>2</sub>). Catalysts synthesized according to that approach are UK63, UK65, and DAL900C. The first two are already listed under approach i.

The fourth approach (iv) uses a metal salt as the exclusive metal precursor and NH<sub>3</sub> under pyrolysis as the exclusive N precursor. The C precursors are carbon black. The catalysts made with this approach are FC280 and M786.

**II.2. RDE. II.2.1. Materials.** Measurements are made at room temperature and atmospheric pressure. The reference electrode is a saturated calomel electrode (SCE) and the counter electrode is a Pt wire. For the Pt/C catalyst, the SCE has a double junction. The electrolyte is an aqueous solution of pH 1 of H<sub>2</sub>SO<sub>4</sub> or HClO<sub>4</sub> for NNMC or Pt/C, respectively. It was checked for some NNMCs that both electrolytes resulted in the same activity,

concurring with the results found in ref 68. Pt nanoparticles (46 wt %) on Vulcan XC-72 (labeled Pt/C) from Tanaka Kikinokoku serve as state-of-the-art Pt catalyst. They have a specific area of 80 m<sup>2</sup> g<sub>Pt</sub><sup>-1</sup> (13).

**II.2.2. Ink Formulation. NNMC.** The ink formulation is (except for CoTMPP700) 10 mg of catalyst, 95 μL of 5 wt % Nafion in alcohol (Aldrich), and 350 μL of ethanol. The ink is prepared in a 5-mL glass vial, shaken for 15 min, and then ultrasonicated for 15 min. This cycle is then repeated twice. A 7-μL aliquot of ink is dropped onto the glassy carbon support (0.196 cm<sup>2</sup>). The 7-μL aliquot results in a catalyst loading of 800 μg cm<sup>-2</sup>. For catalysts UK63 and UK65 only, a 4-μL aliquot is used for reasons explained in section III.

Other ink formulations were tested on a case-by-case basis and, except for CoTMPP700, resulted in equal or lower mass activity than with the above ink (Supporting Information, section C). For CoTMPP700, the ink formulation (defined by the University of New Mexico) consists of preparing two solutions: solution 1 (10 mg of NNMC and 1 mL of deionized H<sub>2</sub>O) and solution 2 (100 μL of a 5 wt % Nafion solution and 1 mL of deionized H<sub>2</sub>O). The final ink is prepared by mixing 400 μL of solution 1 with 80 μL of solution 2 and adding 1520 μL of deionized H<sub>2</sub>O. A 30-μL aliquot is dropped on the disk, resulting in a loading of 306 μg cm<sup>-2</sup>.

**Pt/C.** The ink formulation is 5 mg of catalyst (mass Pt and C), 40 μL of 5 wt % Nafion in alcohol, 222 μL of ethanol, and 10 μL of distilled H<sub>2</sub>O. The ink is then mixed as described above for the usual NNMC ink. Then, a 7-μL aliquot is dropped on the glassy carbon, resulting in a catalyst loading of 657 μg (mass Pt and C) cm<sup>-2</sup>.

**II.2.3. Voltammetry.** For Pt/C, Pt is cleaned by cycling 20 times from –0.2 to +0.8 V vs SCE at 50 mV s<sup>-1</sup> while the electrode is idle. Then, for NNMC and Pt/C alike, one cycle in an O<sub>2</sub>-saturated electrolyte is recorded starting with an idle electrode at –0.25 V vs SCE and up to +0.75 V vs SCE, at which point the electrode is rotated at 1500 rpm. The scan rate is 10 mV s<sup>-1</sup>. The scan from +0.75 to –0.25 V vs SCE under 1500 rpm is the raw data from which the ORR activity is extracted. N<sub>2</sub> is then bubbled into the solution. The capacitive current *I*<sub>CAP</sub> is measured between –0.25 and +0.75 V vs SCE at 10 mV s<sup>-1</sup>.

**II.2.4. Corrections for Capacitive Current and O<sub>2</sub> Diffusion Limitation.** The current density, *I* (A cm<sup>-2</sup>), during the downward scan in the O<sub>2</sub>-saturated electrolyte is corrected by subtracting *I*<sub>CAP</sub> to yield the Faradaic current density, *I*<sub>F</sub> = *I* – *I*<sub>CAP</sub>, defined as negative for a reduction reaction. Next, it is possible to calculate from *I*<sub>F</sub> the current that would be measured if O<sub>2</sub> diffusion were infinitely fast. That current is the kinetic current, *I*<sub>K</sub>, and is, for a given loading, controlled only by the ORR kinetics of the catalyst. The relationship between *I*<sub>K</sub> and *I*<sub>F</sub> is the Koutecky-Levich equation *I*<sub>K</sub> = –*I*<sub>F</sub>*I*<sub>lim</sub>/(*I*<sub>F</sub> – *I*<sub>lim</sub>) (ref (99), p 290). *I*<sub>K</sub> is in A cm<sup>-2</sup> and defined as <0 for a reduction while *I*<sub>lim</sub> is the limiting current density. The *I*<sub>lim</sub> value was taken from the *I*<sub>F</sub> value at –0.25 V vs SCE.

**II.2.5. Definitions of NNMC Mass Activity and Pt/C Mass Activity.** In order to allow for a comparison with previously reported mass activities of NNMCs, the mass activity defined by eq 1 is reported in section III. Volumetric activities as defined in the Introduction are reported in the Discussion section. The ORR mass activity of a C-based NNMC is defined by

$$I_M(\text{NNMC}) = -I_K/m_{\text{catalyst}} [\text{A g}^{-1}] \quad (1)$$

where *I*<sub>M</sub> > 0 and *m*<sub>catalyst</sub> is the NNMC loading on the glassy carbon (g cm<sup>-2</sup>). The potential at which the *I*<sub>M</sub> value is reported is 0.8 V vs a reversible hydrogen electrode (RHE), as chosen in ref 13. The mass activity of the Pt/C catalyst is similarly defined by

$$I_M(\text{Pt/C}) = -I_K/m_{\text{carbon}} [\text{A g}^{-1}] \quad (\text{II})$$

where  $m_{\text{carbon}}$  is the carbon loading contained in the Pt/C film. Defining the mass activity of Pt/C by eq II allows a direct comparison with NNMCM mass activities because both activities are only one step away from the volumetric activity defined in the Introduction, namely, multiplication by the effective density of C in the porous cathode.

**II.2.6. Reference Electrode and Reference Potential.** RDE measurements in the present paper report the potential versus RHE. The change from the SCE to RHE scale is made by measuring the voltage  $\Delta E_{\text{ref}}$  between the SCE and a Pt foil immersed in the same electrolyte saturated in  $\text{H}_2$ .  $\Delta E_{\text{ref}}$  was about  $304 \pm 2$  mV at pH 1.

**II.3. PEM Fuel Cell. II.3.1. MEA Preparation.** The anode catalyst is 40 wt % Pt/C from E-TEK with a loading of  $0.35 \text{ mg Pt cm}^{-2}$  predeposited as a film on top of an ELAT gas diffusion layer (GDL). A circular piece of  $1.14 \text{ cm}^2$  is cut out with a punch. A thin coat ( $0.4\text{--}0.5 \text{ mg of Nafion cm}^{-2}$ ) of a 5 wt % Nafion solution is brushed onto the anode active side. The cathode is prepared by pipetting the required aliquot of catalyst ink on the hydrophobic side of a  $1.14 \text{ cm}^2$  uncatalyzed ELAT GDL (thickness and mass of  $360\text{--}400 \mu\text{m}$  and  $20\text{--}25 \text{ mg cm}^{-2}$ , respectively). The catalyst loading is measured by weighing the dry GDL before and after application of the ink. The mass gain is due to the dry mass of a Nafion ionomer and the mass of the catalyst. Because the ratio of Nafion to catalyst is known, it is possible to deduce the catalyst mass from the mass change. The anode and cathode are dried first on a heat plate and then at  $80 \text{ }^\circ\text{C}$  under vacuum, then weighed, and then hot-pressed at  $140 \text{ }^\circ\text{C}$  against a Nafion 117 membrane (thickness  $160\text{--}170 \mu\text{m}$ , a  $5 \times 5 \text{ cm}$  piece). The anode, cathode, and membrane are placed in a compression set made of two copper plates ( $11 \times 11 \text{ cm}$ ) and of two masks (thickness  $280 \mu\text{m}$ ), with each mask having a  $1.14 \text{ cm}^2$  hole to host the electrodes. One additional mask of thickness  $100 \mu\text{m}$  was added for the cathodes loaded with  $4 \text{ mg cm}^{-2}$  of NNMCM. The press is a Carver laboratory press made of two metal plates ( $15 \times 15 \text{ cm}$ ) heated by cartridges. The compression test is installed in the press, the two heated plates of the press are brought in contact with each face of the set without any load for 1 min, and then a load of 500 lbs (0.4 metric ton) is applied for 40 s. The membrane electrode assembly (MEA) is installed in a fuel-cell fixture of Electrochem Inc., and the experiments are controlled with a potentiostat PARSTAT 2273 (Princeton Applied Research). The MEA is installed so that its  $1.14 \text{ cm}^2$  geometric active area is placed in the middle of the  $5 \text{ cm}^2$  area of serpentine gas channels, and the rest of the MEA (Nafion 117,  $5 \times 5 \text{ cm}$  piece) is clamped between two Teflon gaskets of thickness  $250 \mu\text{m}$ . An additional gasket of  $100 \mu\text{m}$  was added at the cathode side for cathodes with a loading of  $4 \text{ mg cm}^{-2}$  of NNMCM.

**II.3.2. Ink Formulation. NNMCM.** Two ink formulations are defined: one in which the Nafion-to-catalyst mass ratio (Naf/Cat) is 1 (ink a) and the other in which it is 2 (ink b). The formulation of ink a is  $10 \text{ mg}$  of catalyst,  $217 \mu\text{L}$  of Nafion (5 wt % Nafion solution, Aldrich, EW 1000),  $272 \mu\text{L}$  of ethanol, and  $136 \mu\text{L}$  of deionized  $\text{H}_2\text{O}$ . The formulation of ink b is  $10 \text{ mg}$  of catalyst,  $435 \mu\text{L}$  of Nafion,  $54 \mu\text{L}$  of ethanol, and  $136 \mu\text{L}$  of deionized  $\text{H}_2\text{O}$ . After the ink was prepared in a 5-mL glass vial, it was mixed by alternating between 15 min of shaking and 15 min of ultrasonication and repeating this cycle twice. For NNMCM loadings of 1 and  $4 \text{ mg cm}^{-2}$ , aliquots of 71 and  $284 \mu\text{L}$  were deposited on  $1.14 \text{ cm}^2$  GDL (the same aliquots for ink a or ink b).

**Pt/C.** For this catalyst (46 wt % Pt on Vulcan, Tanaka), INRS has studied the effect of various mass ratios of Nafion-to-carbon, Naf/C (unpublished). For our method of preparation and for a  $1.14 \text{ cm}^2$  MEA, the maximum activity was found for Naf/C =

2. The corresponding ink formula is  $10 \text{ mg}$  of Pt/C,  $235 \mu\text{L}$  of Nafion,  $28 \mu\text{L}$  of ethanol, and  $74 \mu\text{L}$  of deionized  $\text{H}_2\text{O}$ . The targeted Pt loading was  $0.33 \text{ mg cm}^{-2}$  ( $28\text{-}\mu\text{L}$  aliquot of ink). The ink was mixed in the same way as that of the NNMCM.

**II.3.3. Experimental Conditions.** Teflon gaskets of thickness 100, 250, or  $500 \mu\text{m}$  are chosen for each MEA so that the average compression of the GDL + active layers is 18–25%. The adjustment of the gasket thickness is important when increasing the cathode loading from 1 to  $4 \text{ mg cm}^{-2}$ . The thickness of the free-standing MEA ( $t_{\text{MEA}}$ ) and of the membrane ( $t_{\text{memb}}$ ) is measured with a micrometer. The former minus the latter gives the sum of the anode and cathode thicknesses (GDLs + active layers), under no compression. The average compression of the anode and cathode in the PEMFC is then

$$\% \text{ compression} = 100(t_{\text{MEA}} - t_{\text{memb}} - t_{\text{gasket}}) / (t_{\text{MEA}} - t_{\text{memb}}) \quad (\text{III})$$

where  $t_{\text{gasket}}$  is the sum of the thickness of the anode and cathode gaskets.

The temperature of the humidifiers and of the cell is raised under  $\text{N}_2$  flow to 100 and  $80 \text{ }^\circ\text{C}$ , respectively. Once the temperatures are stable,  $\text{O}_2$  and  $\text{H}_2$  flows are switched on (208 and  $416 \text{ sccm}$ , respectively, corresponding to  $\sim 90$  times the stoichiometric flow for 1 A), backpressures (gauge pressures) are set to +1 bar (the gas pressure at either the anode or cathode is thus  $1 \text{ atm} + 1 \text{ bar}$ , and the  $\text{O}_2$  and  $\text{H}_2$  partial pressures are 1.5 bar because  $P_{\text{H}_2\text{O,sat}}$  at  $80 \text{ }^\circ\text{C}$  is 0.5 bar), and the cell voltage is set to 0 V for about 5 min (for measurement with NNMCM only) to completely humidify the membrane. Then, the cell is allowed to set at open-circuit potential (OCP) until the OCP stabilized. Then the polarization curve of the NNMCM is recorded by scanning the cell voltage from 0.9–0.85 V down to 0.1 V at a scan rate of  $0.5 \text{ mV s}^{-1}$ . Immediately after, an electrochemical impedance spectroscopy (EIS) measurement is taken at the OCP. Then, cyclic voltammetry under  $\text{N}_2$  at the cathode is recorded for all NNMCM MEAs: the cell is allowed to cool at room temperature, and the humidifier temperatures are set to  $60\text{--}70 \text{ }^\circ\text{C}$ ; the anode and cathode backpressures are both +1 bar. At the anode,  $\text{H}_2$  is diluted with  $\text{N}_2$ , and at the cathode, pure  $\text{N}_2$  is used. Cyclic voltammetry is performed between 0.0 and 1.2 V with a scan rate of  $20 \text{ mV s}^{-1}$ .

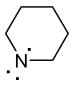
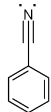
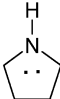
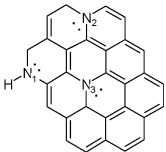
For the Pt/C catalyst, the cathode is activated by a breakin at 0.6 V for 5 h, followed by repeating 5 times the following cycle: 0.85 V for 15 min/OCP for 15 min/0.65 V for 15 min. The polarization curve is recorded with a scan rate of  $0.5 \text{ mV s}^{-1}$  immediately after the last step at 0.65 V.

**II.3.4. iR Correction with EIS.** Because the  $\text{H}_2$  oxidation reaction is fast over Pt, the anode overpotential is less than 10 mV (28) and the cell voltage is about the cathode potential,  $E_c$  (V vs RHE), minus the ohmic drop,  $|I|R$ . The value  $R$  is measured with EIS. For cathodes loaded with  $1 \text{ mg cm}^{-2}$  of NNMCM, the  $R$  values were  $180\text{--}230 \text{ m}\Omega \text{ cm}^2$  except for cathodes made with the catalysts DAL900A and DAL900C ( $300 \text{ m}\Omega \text{ cm}^2$ ) and with CoTMPP700 ( $390 \text{ m}\Omega \text{ cm}^2$ ).

**II.4. Catalyst ex Situ Characterization. II.4.1. NAA and XPS.** NAA is used to assess the bulk concentration of the metals and is performed at Ecole Polytechnique de Montreal. Surface elemental analysis is done by XPS using a VG Escalab 200i instrument and a Al  $K\alpha$  line (1486.6 eV) as the X-ray source. The N 1s narrow scan is deconvoluted in five peaks (Table 1), one each for a N type except peaks II and III. Peaks II and III may each be a lump response of two N functionalities. All peak functions are 30% Gaussian and 70% Lorentzian. Constraints on the peak position and width are applied (Table 1).

The various N coordinations with the C support have been presented in refs 100–102. Except for graphitic N in the

**Table 1. Constraints Applied to the Centers and Width of the Gaussian–Lorentzian Functions for Fitting of the Experimental N XPS Narrow-Scan Spectrum**

Peak	I	II	III	IV	V
Nitrogen type	Pyridinic	Nitrile or Me-N <sub>x</sub>	Pyrrolic or graphitic-N <sub>1</sub> -position	Graphitic	Oxidized
Binding energy / eV	397-399.5	399-400.5	400.2-400.9	401-403	402-405
FWHM / eV	1-1.1	1-1.1	1-1.1	1-1.1	1-4
Atomic environment					
Electron orbitals	4e sp <sup>2</sup> (1 lone pair) 1e p (π-system)	2e p 3e sp (1 lone pair)	3e sp <sup>2</sup> 2e p (π-system)	3e sp <sup>2</sup> 2e p (π-system)	

position N<sub>3</sub> (see the scheme corresponding to peak IV in Table 1), all N types are found at the edge of graphene layers (Table 1). Graphitic N bonded to three C atoms has a binding energy (BE) of 400.5–402.7 eV, while when bonded to two C atoms and one H atom (position N<sub>1</sub>, Table 1), it has a BE of 400.1–401.2 eV (101). This lower BE overlaps with the BE ascribed to pyrrolic N. Thus, peak III must be regarded as the sum of pyrrolic N and graphitic N of type N<sub>1</sub> (101). Peak II must also be regarded as a sum, namely, that of nitrile N and N bonded to a metal in an Me–N<sub>x</sub> center. The assignment to the Me–N<sub>x</sub> type of N is based on studies of metal-less and metal-containing macrocycles. The replacement of protons by a metal ion introduces an electron-withdrawing effect, leading to an increase in the N 1s BE (103, 104). Studies of iron and cobalt porphyrins have reported a N 1s BE of ~399.2 eV (93–96).

**II.4.2. N<sub>2</sub> Isotherm and Its Analysis.** Measurements are made with a Quantachrome Instruments Autosorb-1. The pore-size distribution (PSD) is determined from the adsorption isotherm using nonlocal density functional theory (NLDFT). In view of the importance of micropores for the present NNM (Discussion section), the correct quantification of micropores is paramount. An NLDFT model specific for disordered carbonaceous materials has been used. Its advantage against the classical slit pore model is now discussed.

The NLDFT was developed for micro-mesoporous materials by Tarazona and co-workers (105, 106) and applies molecular simulations to bulk fluids or fluids confined in pores. The PSD analysis (107–109) is based on a set of local adsorption isotherms (kernel), with each local isotherm being calculated for a given pore width. The task is to determine the contribution of each kernel to the experimental isotherm. This deconvolution task is usually solved by the Tikhonov regularization procedure (110). Nowadays, this NLDFT-based PSD analysis is found in softwares of automatic analyzers produced by Micromeritics Instruments and Quantachrome Instruments. However, the theoretical basis was developed for crystalline surfaces like graphite while activated carbon or carbon black shows a different type of pore surface (111). The model proved imperfect for carbon powders, which appeared in poor fitting of the experimental adsorption isotherms. As a result, the PSD often shows a gap around the pore size of 1 nm, which is a model-generated artefact (112). To improve the situation, it was necessary to extend the NLDFT to amorphous solids, accounting for surface roughness and energetic heterogeneity. This has

been done with a new concept that considers the solid and adsorbed gas as two components of a binary mixture (112–115). The gas–solid molecular parameters were determined by fitting a N<sub>2</sub> adsorption isotherm of a nongraphitized carbon black BP 280 Cabot (111). The fitting error was <2% over 6 orders of magnitude of pressure, proving that the new model accounts for the energetic heterogeneity of amorphous surfaces. In the present work, the newly developed NLDFT is relied on to analyze the PSD of the catalysts. If one would have used the classical NLDFT model found in commercial softwares instead, the conclusion of the importance of micropores for the activity of such catalysts would not change. However, the fine subdivision of micropores made in Figure 11 would have been impossible.

### III. RESULTS OF ORR MASS ACTIVITY IN RDE

Figure 1A presents the Faradaic current density,  $I_F$ , of the various NNMCs and of the Pt/C catalyst, measured at a rotation of 1500 rpm. The target NNMC curves, curves b in Figure 1A,B, are derived from the Pt/C Tafel plot (curve a in Figure 1B), as explained in the Supporting Information, section D. The target NNMC curve has the same Tafel slope as Pt/C and one-tenth of the Pt/C mass activity,  $I_M$  (eq II). The mass activity measured for Pt at 0.9 V (Figure 1B) is about 65 A (g of C + Pt)<sup>-1</sup>, i.e., about 140 A g<sub>Pt</sub><sup>-1</sup> at 20 °C. This value is close to values reported for the very same catalyst in Table 4 of ref 13 (160–220 A g<sub>Pt</sub><sup>-1</sup> at 60 °C).

For UK63 and UK65, the loading was decreased from 800 to 460 μg cm<sup>-2</sup>. The loading of 800 μg cm<sup>-2</sup> resulted in two drawbacks: (i) a large spike at 0.75 V vs RHE and (ii) the reading of the mass activity at 0.8 V vs RHE required extrapolation of the Tafel slope observed at  $E > 0.8$  V vs RHE.

For a 4e ORR reduction at 1500 rpm, a limiting current of ~6 mA cm<sup>-2</sup> is expected. A flat plateau is observed for the catalysts Pt/C, UK63, UK65, FC280, and M786 (Figure 1A). The other catalysts show a tilted plateau and a transition of control from kinetics to diffusion that is not as sharp as that for the catalysts previously mentioned (except DAL900C, with a sharp transition but tilted plateau). This could be due

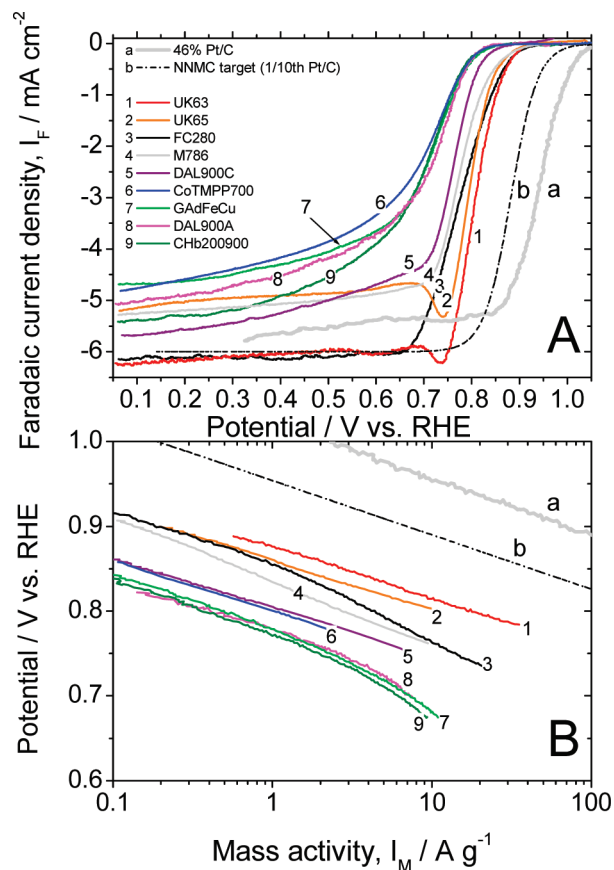


FIGURE 1. (A) Polarization curves in RDE at 1500 rpm.  $O_2$ -saturated electrolyte of pH 1 at 20 °C. NNMC loading of  $800 \mu\text{g cm}^{-2}$  except UK63-65 ( $460 \mu\text{g cm}^{-2}$ ) and CoTMPP700 ( $306 \mu\text{g cm}^{-2}$ ). Curve a: Pt/C,  $302 \mu\text{g}$  of Pt  $\text{cm}^{-2}$  ( $355 \mu\text{g}$  of C  $\text{cm}^{-2}$ ). Curve b: NNMC target for year 2010 for a loading of  $460 \mu\text{g cm}^{-2}$ . Other curve labels are 1 (UK63), 2 (UK65), 3 (FC 280), 4 (M786), 5 (DAL900C), 6 (CoTMPP700), 7 (GAdFeCu), 8 (DAL900A), and 9 (Chb200900). (B) Tafel plots ( $E$  vs  $\log I_M$ ) in RDE. Same conditions as those in part A. Curve a: 46% Pt/C. Curve b: NNMC target by U.S. DOE for year 2010. For curve a, the Pt activity is as defined by eq II [ $A (\text{g of C})^{-1}$  contained in Pt/C].

to the restricted porosity inside the catalytic film, leading to  $O_2$  diffusion limitation not only in the quiescent electrolyte layer close to the electrode but also inside the porous catalytic film. Possibly, the tilted plateau arises because  $O_2$  is not fully reduced to  $H_2O$  on these particular NNMCs. Measurement of %  $H_2O_2$  was not made because it is more complex than previously believed. It has been recently shown for an NNMC synthesized by Fe impregnation, like FC280, that %  $H_2O_2$  decreases dramatically with an increase in the catalyst loading (116). This has also been observed for a Ru–Se catalyst (117).

Figure 1B presents the kinetically controlled current  $I_M$  of various NNMCs and of the Pt/C catalyst. Tafel slopes are observed for all NNMCs in the interval 0.9–0.75 V vs RHE with values in the range 54–65  $\text{mV decade}^{-1}$  except for M786 (77  $\text{mV decade}^{-1}$ ). The mass activities at 0.8 V vs RHE obtained from Figure 1B are reported later.

Figure 2A presents the  $N_2$  cyclic voltammograms ( $N_2$ -CVs) in RDE recorded at a scan rate of  $10 \text{ mV s}^{-1}$ . The signal is expected to depend on the specific surface area of the catalysts but might also depend on the quality of the electrolyte–catalyst interface. Catalyst UK65 shows a redox

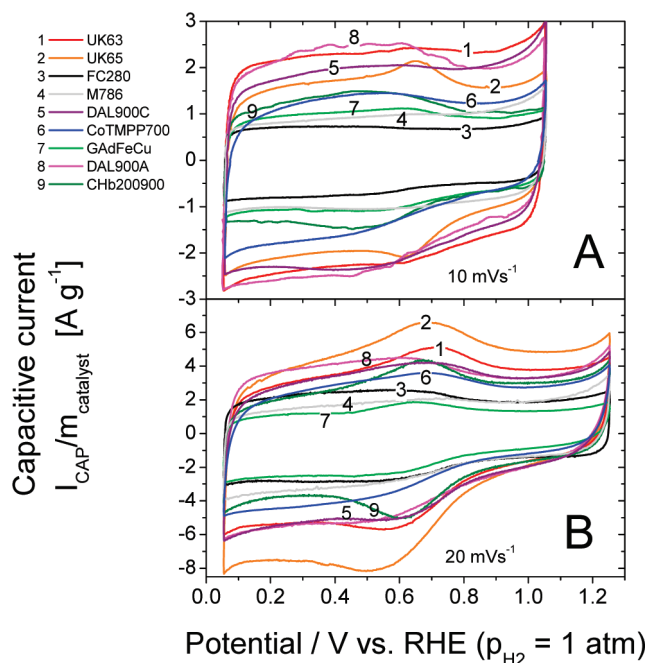


FIGURE 2. (A)  $N_2$  cyclic voltammetry in RDE.  $N_2$ -saturated electrolyte of pH 1. Scan rate  $10 \text{ mV s}^{-1}$ . Curve labels are 1 (UK63), 2 (UK65), 3 (FC 280), 4 (M786), 5 (DAL900C), 6 (CoTMPP700), 7 (GAdFeCu), 8 (DAL900A), and 9 (Chb200900). (B)  $N_2$  cyclic voltammetry of the NNMC cathodes in PEMFC. Scan rate  $20 \text{ mV s}^{-1}$ , Naf/Cat ratio 2, and NNMC loading  $1 \text{ mg cm}^{-2}$ .

peak. The nature of the redox peaks is discussed in the Supporting Information, section E. The  $N_2$ -CVs measured under PEMFC conditions (Figure 2B) and at a scan rate of  $20 \text{ mV s}^{-1}$  are discussed in the next section.

## IV. PEMFC RESULTS

**IV.1. ORR Mass Activity.** PEMFC polarization curves are shown only in the next section because graphs of the potential versus the current in a linear scale cannot display the ORR mass activity at 0.8 V vs RHE (small currents). The first figure of this section presents the Tafel plots of the various NNMCs and of Pt/C (Figure 3). For each NNMC, PEMFC experiments were conducted with two possible Nafion-to-catalyst mass ratios in the cathode ink (Naf/Cat of 1 or 2) and with two possible NNMC loadings at the cathode (1 or  $4 \text{ mg cm}^{-2}$ ). Figure 3 presents only the Tafel plots obtained with Naf/Cat = 2 and a loading of  $1 \text{ mg cm}^{-2}$ . It will be seen later that, for any NNMC, this combination resulted in the highest ORR mass activity. The ORR mass activity at 0.8 V vs RHE ( $iR$ -corrected potential) is either directly read when the curve shows a straight Tafel slope at 0.8 V or, for catalysts UK63, UK65, M786, and DAL900C, is obtained by extrapolation of the Tafel slope seen at potentials  $>0.8 \text{ V}$ . Such an extrapolation is shown for M786 and also for the Pt/C catalyst (dash-dotted lines in Figure 3). The ORR mass activities thus obtained are reported later in this section.

The targeted Tafel plot for NNMC by year 2010 according to the U.S. DOE (one-tenth of the Pt/C activity) is represented by curve b and was calculated from the experimental Pt/C curve a in the same manner as that in section III. A Tafel slope of  $65 \text{ mV decade}^{-1}$  is assumed, and the targeted mass

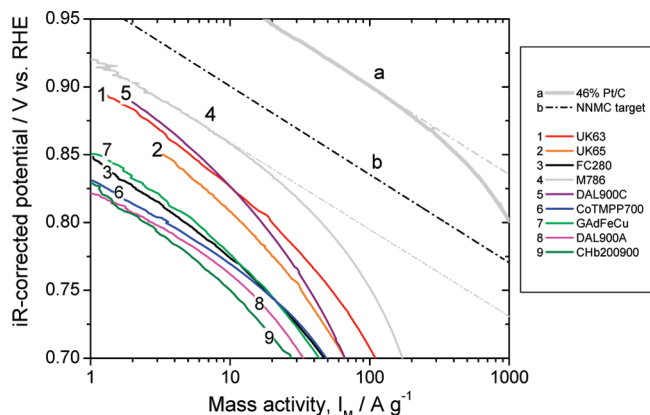


**FIGURE 3.** Tafel plots of the various NNMC cathodes in a PEMFC. NNMC loading  $1 \text{ mg cm}^{-2}$ . Naf/Cat = 2. Curve a: 46% Pt/C;  $0.33 \text{ mg of Pt cm}^{-2}$ ; Naf/Cat = 2. For curve a, the Pt activity is as defined by eq II [ $\text{A (g of C)}^{-1}$  contained in Pt/C]. Curve b: estimated target activity for NNMC for year 2010 (see the Supporting information, section D).

activity is one-tenth of that measured on Pt/C in the same PEMFC and under the same conditions.

Figure 2B reports the  $\text{N}_2$ -CVs (scan rate  $20 \text{ mV s}^{-1}$ ) measured in situ in a PEMFC on the same MEAs whose Tafel plots are reported in Figure 3.  $\text{N}_2$ -CVs in a PEMFC on cathodes having other combinations of Naf/Cat ratios and NNMC loadings were measured as well but are not shown. The catalysts UK63, UK65, and CHb200900 show a clear redox peak.

Generally, the NNMCs show more intense redox peaks in a PEMFC than in a RDE (e.g., UK63). This is particularly true at a loading of  $4 \text{ mg cm}^{-2}$  (not shown). This does not seem to be due to a better covering of the catalyst surface by the Nafion ionomer in the PEMFC cathodes than in the RDE ones because the capacitance per mass of catalyst (values reported later) is generally not much larger in a PEMFC than in a RDE and sometimes even smaller. Maybe the pH of the Nafion ionomer is  $< 1$ . This could lead to more intense redox peaks in PEMFC vs RDE because the Supporting Information, section E, shows that the redox signal increased when the pH decreased from 4 to 1.

Next, Figure 4A reports, for each catalyst, the ORR mass activities at  $0.8 \text{ V vs RHE}$  in RDE and in PEMFC. The x axis lists the NNMCs according to increasing RDE mass activity. Considering all catalysts, the activity in a RDE spans from  $0.4$  to  $18 \text{ A g}^{-1}$  while the activity in a PEMFC spans from  $0.7$  to  $80 \text{ A g}^{-1}$ . Three remarks are made:

(i) For each catalyst, the mass activity is usually higher in a PEMFC than in a RDE. For example, M786 shows a factor of 7.5–28 higher activity in PEMFC than in RDE. Only FC280, UK65, and UK63 show similar activities in PEMFC and RDE.

(ii) For each catalyst, the mass activity is highest with a ratio Naf/Cat of 2.

(iii) At a fixed ratio Naf/Cat of 2, an increase in the loading from  $1$  to  $4 \text{ mg cm}^{-2}$  resulted in slightly improved mass activity (FC280), slightly decreased mass activity (CHb200900, DAL900C, UK65, and UK63), or a decrease by a factor of about 2 (DAL900A, GAdFeCu, CoTMPP700, and M786).

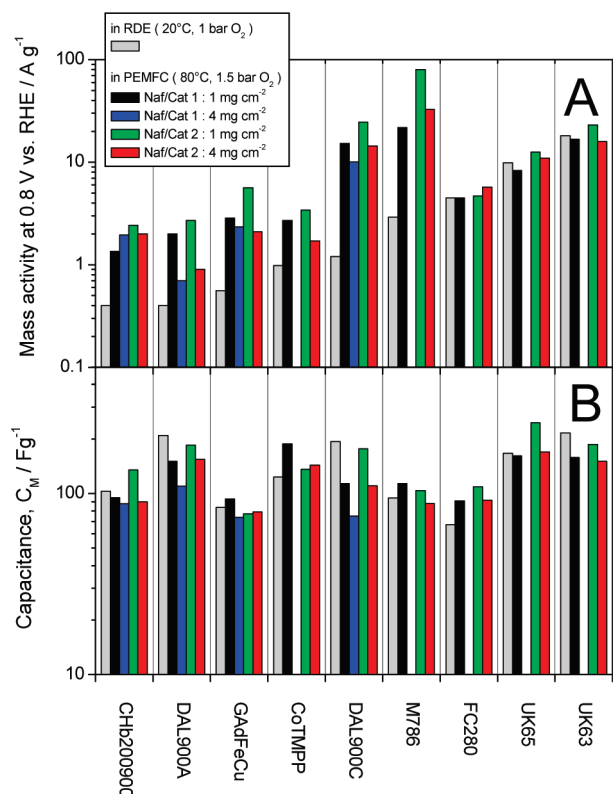


**FIGURE 4.** (A) ORR mass activity at  $0.8 \text{ V vs RHE}$  in RDE and PEMFC. (B) Capacitance in RDE and PEMFC.

In order to explain why, for a given NNMC, the mass activity may show large changes from RDE to PEMFC (remark i above), one might call upon two phenomena: (a) the extent of the interface Nafion ionomer/NNMC or (b) the activation energy that governs the increase in activity with temperature ( $60 \text{ }^\circ\text{C}$  increase from RDE to PEMFC).

The temperature effect was *not* experimentally investigated for all catalysts at intermediate temperatures and will only be examined in the Discussion section. Point a is now investigated by analyzing the  $\text{N}_2$ -CVs measured in RDE and PEMFC. The capacitance is averaged over one full cycle according to

$$C_M = \frac{\int I_{\text{CAP}} dE}{m_{\text{catalyst}} \times 2\nu\Delta E} \quad [\text{F g}^{-1}] \quad (\text{IV})$$

where  $C_M$  is the average capacitance per mass of catalyst,  $I_{\text{CAP}}$  is the capacitive current density,  $E$  is the potential,  $m_{\text{catalyst}}$  is the catalyst loading,  $\nu$  is scan rate, and  $\Delta E$  is the scanned potential window.

Figure 4B presents the  $C_M$  values under RDE and PEMFC conditions. For each catalyst, we now investigate whether changes in the  $C_M$  values could explain some of the large changes observed in the  $I_M$  values when switching from RDE to PEMFC. When parts A and B of Figure 4 are compared, it is obvious that the increased activity in PEMFC vs RDE activity (e.g., GAdFeCu, DAL900C, and M786) cannot be explained by an improved Nafion–catalyst interface because the average capacitance in a PEMFC is only negligibly

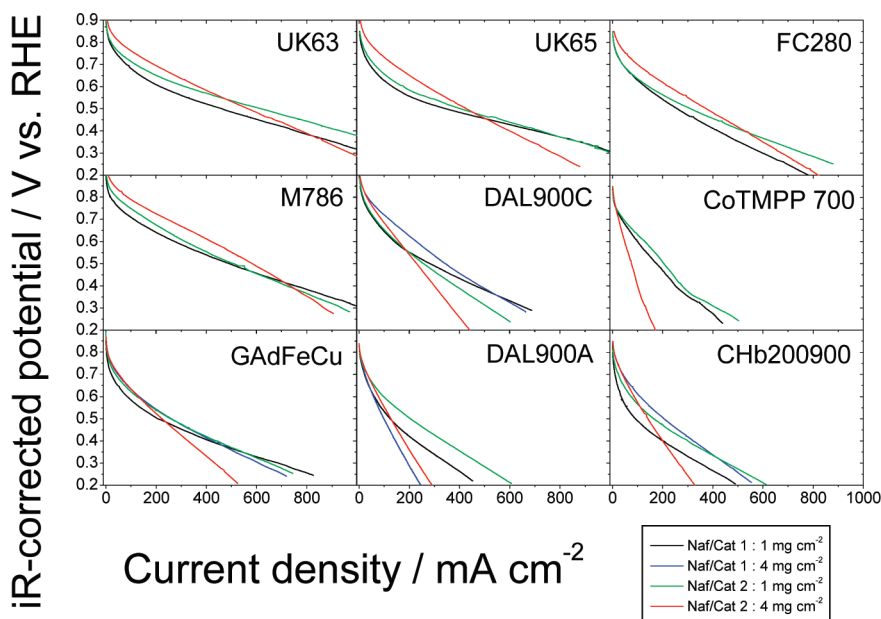


FIGURE 5. Cathode polarization curves of all NNMCs in the PEMFC. Each color corresponds to a given set of mass ratio Nafion/NNMC (Naf/Cat) in the cathode and of NNMC loading at the cathode. Black: Naf/Cat mass ratio = 1 and NNMC loading  $1 \text{ mg cm}^{-2}$ . Blue: Naf/Cat = 1 and NNMC loading  $4 \text{ mg cm}^{-2}$ . Green: Naf/Cat = 2 and NNMC loading  $1 \text{ mg cm}^{-2}$ . Red: Naf/Cat = 2 and NNMC loading  $4 \text{ mg cm}^{-2}$ .

higher in PEMFC versus that in RDE (M786) or even smaller (GAdFeCu and DAL900C).

The other alternative to account for this effect of improved activity in PEMFC versus RDE for some catalysts would be a temperature effect (see the Discussion section).

**IV.2. Fuel Cell Performance.** While the previous section focused on the mass activity of NNMCs under kinetic control, here we are interested in the current density ( $\text{mA cm}^{-2}$ ) of the porous cathode and how it can be maximized by either increasing the catalyst loading (costless) or optimizing the ink recipe. In the present work, NNMC cathodes are fabricated onto a GDL, which is then hot pressed against the membrane. We recognize that this procedure, although adapted for measurement on  $1 \text{ cm}^2$  MEA, is probably not the best fabrication method especially for MEAs  $>5 \text{ cm}^2$ . For example, for the catalyst CoTMP700, an alternative MEA fabrication yielded an equal or slightly better performance than that reported here (92, 93). This being pointed out, the performance of the various catalysts with the present fabrication method is now compared.

Figure 5 presents all PEMFC polarization curves. At a fixed loading of  $1 \text{ mg cm}^{-2}$ , it is seen that the Naf/Cat ratio of 2 (green curves) resulted for all NNMCs in an equal or higher performance than that of the Naf/Cat ratio of 1 (black curves) at all potentials, except for DAL900C, for which these two curves cross each other at 0.6 V. Next, at a fixed Naf/Cat ratio of 2, increasing the loading from 1 to  $4 \text{ mg cm}^{-2}$  usually resulted in a higher performance at high potential, while at low potential, the performance was poorer (green vs red curves). The intersection point of these two curves depends greatly on the NNMC. For a given NNMC, the fact that the PEMFC polarization curve with high loading crosses that with low loading can be explained on theoretical grounds by modeling of the porous cathode. For example, simultaneous limitation by proton and electron conduction

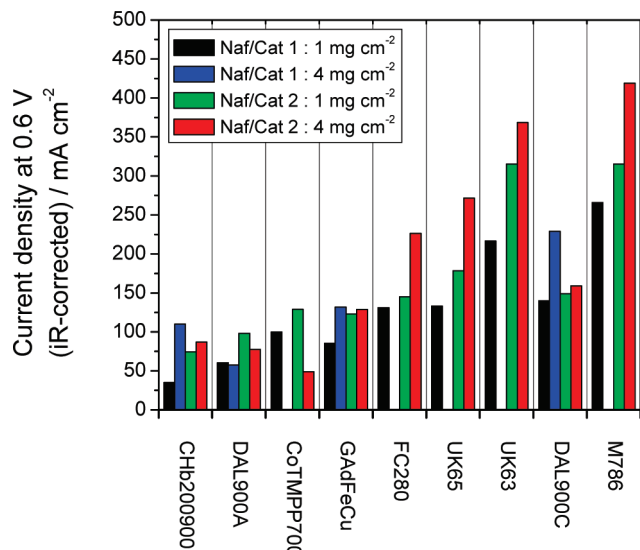


FIGURE 6. Current density at 0.6 V (*iR*-corrected) in PEMFC. The catalysts are ranked from left to right by increasing mass activity at 0.8 V in PEMFC.

inside any porous electrode yields such an effect. Water flooding combined with another transport limitation might also result in such an effect. However, such a modeling example is not known by the authors to have been reported in the literature.

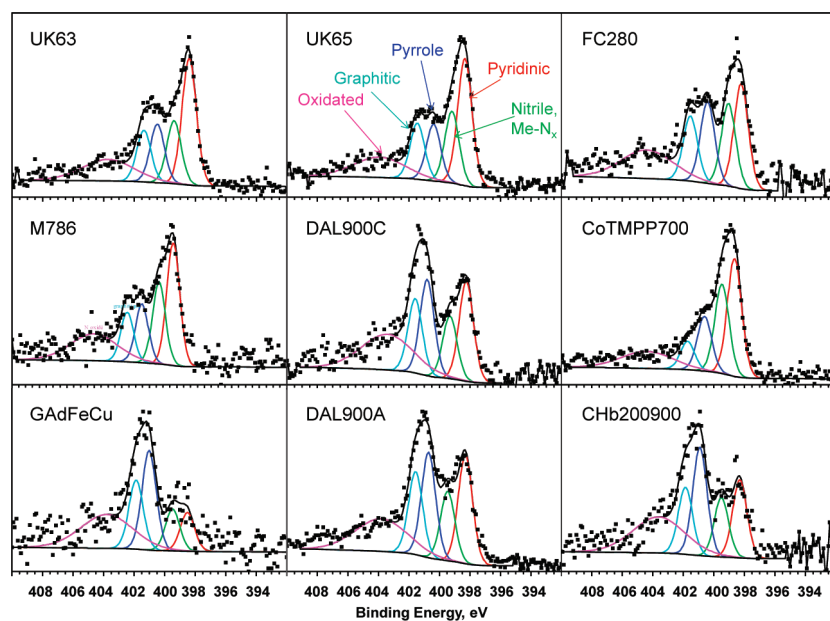
For practical applications of the PEMFC, the operating voltage would likely not be  $<0.6 \text{ V}$  because otherwise the energy efficiency is too low and the heat production too high. Thus, the *iR*-corrected cell voltage of 0.6 V was chosen in order to compare the current density of all NNMC cathodes (Figure 6). The *x* axis ranks the NNMCs according to mass activity at 0.8 V in the PEMFC. Thus, if all NNMC cathodes had identical mass- and charge-transport properties, the current density at 0.6 V should increase from left to right. Obviously, this is not necessarily the case, especially not for



**Table 2. Elemental Surface (XPS) and Metal Bulk (NAA) Concentrations of the NNMCs<sup>a</sup>**

	N <sub>total</sub>	N <sub>pyridinic</sub>	N <sub>nitrile or Me-N<sub>x</sub></sub>	N <sub>pyrrolic</sub>	O	metal	Si	S	metal bulk
UK63	3.06	1.03	0.51	0.47	3.50	0.36 Fe		0.45	0.71 Fe
UK65	2.55	0.84	0.47	0.38	2.64	0.30 Fe		0.19	0.08Co 0.62 Fe
FC280	1.90	0.45	0.36	0.35	0.49	<0.1 Fe			0.06 Fe
M786	1.91	0.57	0.38	0.28	1.31				0.17 Fe
DAL900C	2.93	0.63	0.40	0.61	1.30	0.12 Fe			0.31 Fe
CoTMPP700	5.37	1.80	1.37	0.83	10.30	0.74 Co 0.30 Fe	0.85		1.29Co 0.14 Fe
GAdFeCu	1.02	0.11	0.11	0.27	2.74	0.48 Cu			0.02Cu 0.15 Fe
DAL900A	3.26	0.74	0.47	0.71	2.46	<0.1 Fe	0.13		0.10 Fe
CHb200900	1.30	0.23	0.17	0.32	5.75				0.26 Fe

<sup>a</sup> Catalysts are listed according to the RDE activity (highest activity on the upper line). All concentrations are given in atom %. Bulk metal content on the last column (atom % bulk).

**FIGURE 7. N 1s narrow scan spectra of the NNMCs and their deconvolution.**

DAL900C. All NNMC cathodes are strongly limited by mass transport at 0.6 V because none of them display an increase by a factor of 4 in the current density when the loading is increased from 1 to 4 mg cm<sup>-2</sup>. Today's harsh transport limitation within the NNMC cathodes is a main barrier to the efficient implementation of NNMC into PEMFC. The cathodes with least poor transport properties are those made with M786, UK63, UK65, and FC280. Two of these catalysts are made from a fine carbon black support, and the two others have high porosity and fine particles (see the Supporting Information, section F) because of the addition of a foaming agent in their synthesis. The poorest mass transport is observed on cathodes made with CHb200900, DAL900A, CoTMPP700, and DAL900C. The last three catalysts involve a silica template in their synthesis, and SEM micrographs show large particles or flakes. Possibly the tortuosity of the electron and/or proton path is higher in these NNMC cathodes.

## V. XPS RESULTS

The elemental surface concentrations of the NNMCs are found in Table 2. For N, the contributions of pyridinic, nitrile, and pyrrolic N atoms are detailed because some of these N types are likely to be involved in the active sites. Figure 7 shows N 1s spectra of the various NNMCs and their deconvolution by five peaks (see section II.4.1).

The N surface content for all NNMCs is 1.30–5.37 atom %. The N functionalities are not divided in the same way for all catalysts. Some show a predominance of pyridinic N (UK63, UK65, FC280, M786, and CoTMPP700) and others an equal repartition between pyridinic and pyrrolic N (DAL900C and DAL900A), while still others show a predominance of pyrrolic N (GAdFeCu and CHb200900).

The O content is in the range 0.49–5.75 atom % except for CoTMPP700 (10.3 atom %). O is chemically or physically adsorbed on the NNMCs upon exposure to air. For some NNMCs, O might also originate from the precursor mol-

ecules. There is no correlation between the O content and NNMC activity.

Next, the surface Fe could be quantified on several catalysts. One interesting point is that the surface Fe is detected only in traces (<0.1) on DAL900A but quantified to 0.12 atom % on DAL900C. The latter is obtained from the former by doing a second heat treatment under  $\text{NH}_3$ , and we saw that this resulted in much improved activity in PEMFC (factor 8).

Next, Si is present on DAL900A and CoTMPP700 and comes from the Si template used in their synthesis. Fluoride is present only on DAL900A and comes from the HF leaching used to remove the Si template.

S is present on UK65 and UK63 and comes from their synthesis (Supporting Information, section B). S prevents excess Fe from forming iron carbide during the heat treatment because excess Fe will preferentially form iron sulfide,  $\text{Fe}_{1-x}\text{S}$ . The formation of iron carbide during the heat treatment of the iron porphyrin would catalyze a long-range graphitization of the C and would negatively affect the surface area of the powder (84, 91).

## VI. NEUTRON ACTIVATION RESULTS

The metal bulk contents of the NNMCs are found in the last column of Table 2. The Fe bulk content is in the range of 0.06–0.71 atom % (0.29–3.3 wt %). CoTMPP700 is mainly Co-based, while catalyst UK65 contains a minor amount of Co. Because the mass activity of Co-based catalysts has been shown for one type of catalyst to be about 10 times lower than that of Fe (78) and under the assumption that this order of magnitude is valid for the other NNMCs containing both Co and Fe (CoTMPP700 and UK65), it can be stated that all of the presently investigated catalysts owe their activity to Fe, except CoTMPP700. The activity of the latter could equally come from Co and Fe.

Evolution of the catalytic activity with the metal bulk content is analyzed in the Discussion section.

## VII. POROSIMETRY RESULTS

Figure 8A shows that the amount of pores differs widely among the various NNMCs. The shapes of the isotherms are, however, grossly similar and typical of carbonaceous materials comprising all types of pores. The isotherms are of type I at  $P/P_0 < 0.05$ , where filling of the micropores by the adsorbate occurs, and of type II at  $P/P_0$  values  $> 0.05$ , where the slope is indicative of the amount of mesopores (118). The isotherms were fitted (solid lines) with a model for disordered carbonaceous materials (section II.4.2) and yielded the PSD (Figure 8B). The importance of the pore size for the kinetic activity of such NNMCs is outlined in the Discussion section.

## VIII. SEM RESULTS

SEM micrographs of all catalysts are shown in the Supporting Information, section F. A quick review of these reveals a chasm between FC280 and all other NNMCs of the present study. FC280 is based on a carbon black that shows a particle size of 20–50 nm and agglomerates of such

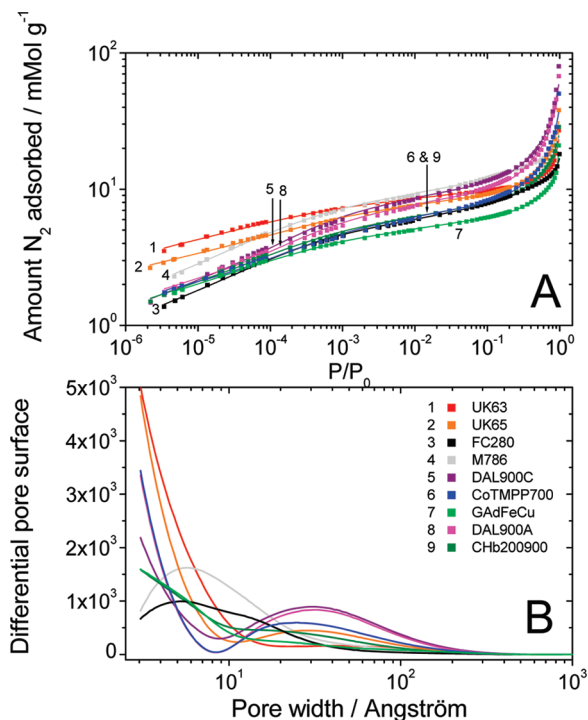


FIGURE 8. (A)  $\text{N}_2$  adsorption isotherms of the various NNMCs. Experiment (squares) and fitting by the present NLDFT model (lines). (B) Surface area distribution obtained from analysis by the present NLDFT model.

particles of about 400 nm. For the other NNMCs (except M786), the carbon structure is entirely formed during the heat treatment because of the partial graphitization of the carbon precursors. These catalysts show a much coarser structure than FC280. The particle size ranges from 0.5 to 20–30  $\mu\text{m}$ . The catalysts UK63 and UK65 have, within that family, a finer structure with average particle sizes of 7 and 4  $\mu\text{m}$ , respectively. This is due to the presence of a foaming agent (iron oxalate) and of S in the preparation of these catalysts. The particle size of such catalysts has been found to be controlled by the crystal size of the iron oxalate used (91, 119). The catalyst M786 is a cross between a carbon black support and a carbon support obtained from graphitization of carbon molecules because its preparation involves 50% of a high-surface-area carbon black and 50% of PTCDA ( $\text{C}_{24}\text{H}_8\text{O}_6$ ). This catalyst shows particles of 3  $\mu\text{m}$  on average.

The existence of large particles ( $> 1 \mu\text{m}$ ) is probably not desirable in a catalytic powder used to form a porous cathode of 10–50  $\mu\text{m}$  thickness. Also, it can be expected that the larger the particle, the more difficult it is for the Nafion ionomer to connect the active sites existing in it. It is also probably more difficult for  $\text{O}_2$  to reach these sites because the pores that exist inside the particles are narrow. Diffusion is much slower in narrow pores because the mechanism changes from molecular (gas–gas collision) to Knudsen (gas–wall collision) diffusion, which can decrease the effective diffusion coefficients by decades. Larger particles might also induce fewer points of contact between the particles and thus might result in a decreased electronic conductivity of the porous cathode.

## IX. DISCUSSION

**IX.1. Volumetric Activity of the Present NNMC Cathodes: Comparison to U.S. DOE Targets.** Equation V converts mass activities at 0.8 V *iR*-free cell voltage,  $I_M$  (defined by eq 1) measured under pressures  $P_{O_2}$  and  $P_{H_2}$  into volumetric activities at 0.8 V *iR*-free cell voltage,  $I_V^*$ , under reference conditions of 1 bar of  $O_2$  and  $H_2$  pressures.

$$I_V^* = I_M \rho_{\text{eff}} \left( \frac{P_{O_2}^*}{P_{O_2}} \right)^{0.79} \left( \frac{P_{H_2}^*}{P_{H_2}} \right)^{\alpha_c/2} \quad (\text{V})$$

where  $P_{O_2}^*$  and  $P_{H_2}^*$  are the reference pressures (1 bar) and  $\rho_{\text{eff}}$  is the effective density of a C-based NNMC in the porous cathode. In eq V, the exponents for  $O_2$  and  $H_2$  pressures have been determined by Neyerlin et al. (eq 12 in ref 120). The coefficient  $\alpha_c$  is the cathodic transfer coefficient and is related to the Tafel slope through  $\alpha_c = RT \ln 10 / (F \times \text{Tafel slope})$ . It is assumed in eq V that the exponent 0.79, determined experimentally for Pt/C, also describes the  $P_{O_2}$  dependence of the activity of NNMCs. Next, the effective density of a C-based NNMC in a porous cathode was previously assumed to be  $0.4 \text{ g cm}^{-3}$  (13). This assumption is retained here. The value of  $0.4 \text{ g cm}^{-3}$  corresponds roughly to 50% porosity in the cathode. Applying eq V, the mass activities at 0.8 V (in  $\text{A g}^{-1}$ ; measured under  $P_{O_2}$  of 1.5 bar, 100% RH, and  $80^\circ\text{C}$ ) multiplied by 0.237 (if  $\alpha_c = 1$ , i.e.,  $70 \text{ mV decade}^{-1}$ ) give the volumetric activities ( $\text{A cm}^{-3}$ ) under the reference conditions ( $P_{O_2}$  and  $P_{H_2}$  of 1 bar, 100% RH, and  $80^\circ\text{C}$ ) defined in refs 13 and 14.

The estimation of the volumetric activities tells us that the two NNMCs presently investigated (UK63, volumetric activity of  $5.6 \text{ A cm}^{-3}$  with  $\text{Naf}/\text{Cat} = 2$ ; DAL900C,  $6.0 \text{ A cm}^{-3}$  with  $\text{Naf}/\text{Cat} = 2$ ) are a factor of 21–23 below the U.S. DOE target of year 2010 ( $130 \text{ A cm}^{-3}$  at 0.8 V) and one catalyst (M786,  $18.7 \text{ A cm}^{-3}$  with  $\text{Naf}/\text{Cat} = 2$ ) is only a factor of 7 below the target. This is a large improvement compared to the volumetric activities of  $0.7\text{--}1.5 \text{ A cm}^{-3}$  under reference conditions (mass activity  $3\text{--}5 \text{ A g}^{-1}$  under 1.5 bar of  $O_2$  pressure) reported for the previous best INRS catalysts (78, 90) that were obtained by impregnation of iron acetate on carbon black followed by heat treatment in  $\text{NH}_3$ . This catalyst type is represented in the present study by FC280 ( $1.1\text{--}1.3 \text{ A cm}^{-3}$ ).

Comparing the present NNMC activities to recent literature data, high activity has also been reached by Wood (88). At  $80^\circ\text{C}$  and under  $O_2/H_2$  backpressures of 50 psig/30 psig, a volumetric activity of  $19 \text{ A cm}^{-3}$  was reported. When the correction for  $P_{O_2}$  and  $P_{H_2}$  (eq V with  $\alpha_c = 1.03$  experimentally determined) is applied, this transforms into  $2.7 \text{ A cm}^{-3}$  under reference conditions ( $P_{O_2}$  and  $P_{H_2}$  of 1 bar).

**IX.2. What Characteristics of NNMC Set Their Activity?** It has been shown that the activity for the ORR is obtained when the simultaneous presence of a metal (Fe and Co), N, and C is ensured during a heat treatment at  $T > 600^\circ\text{C}$ . Recently, it has been shown at INRS, for catalysts synthesized by impregnation of an iron salt onto a non-

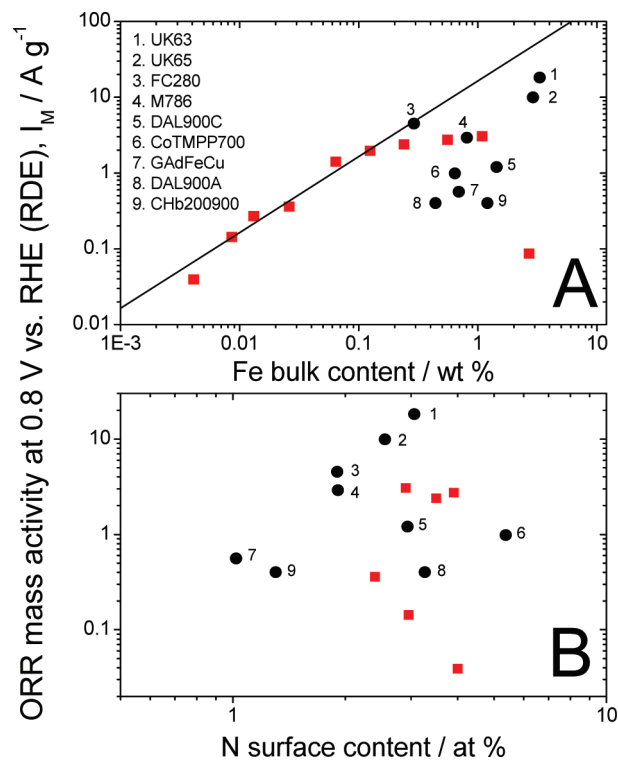


**FIGURE 9.** (A) Mass activity in RDE vs Fe bulk content (measured by NAA) of NNMC. The red squares are literature data obtained by the impregnation of different amounts of Fe on a non-microporous carbon and heat treatment at  $950^\circ\text{C}$  in  $\text{NH}_3$  for the duration necessary to obtain 30–35 wt % loss of C. Red squares reprinted with permission from ref 78. Copyright 2008 Elsevier. (B) Mass activity in RDE vs N surface content (XPS) of NNMC. Red squares reprinted with permission from ref 78. Copyright 2008 Elsevier.

microporous carbon black of low surface area followed by heat treatment with the dried powder at  $950^\circ\text{C}$  in pure  $\text{NH}_3$ , that the activity was controlled by the microporous surface area (pore size  $< 20 \text{ \AA}$ ) produced during the heat treatment (77). Thus, three factors are of particular interest in trying to explain the activity of NNMC: the metal content, the N content, and the microporous area created during the heat treatment.

Figure 9A presents, as a function of the bulk Fe content, the ORR mass activity measured in RDE for the present NNMC (circles) as well as data measured previously (squares) by changing on purpose the Fe content of catalysts synthesized otherwise under fixed conditions (78). In that work, it was observed that the activity increased linearly only up to a Fe content of about 0.1 wt %, where the activity departed from the linear relationship (solid line in Figure 9A). For the squares, the leveling off and decrease of the activity at  $\text{Fe} > 0.1 \text{ wt } \%$  was explained by the concomitant decrease of the microporous area of the catalysts (78). With regard to the very different ways of producing the NNMC of the present data (circles), the superimposition of the new data to the former one (squares) fits surprisingly well. The only catalysts with Fe content  $> 0.1 \text{ wt } \%$  that show increased activity are UK63 and UK65. Their activity is, however, less than predicted by the solid line by a factor 2–4, and this is interpreted as an Fe utilization of 25–50%. A detailed study of similar catalysts is found in ref 84. Their activities were

found to correlate with one structure found in Fe Mössbauer spectroscopy (D1). Only 30–60% of Fe was found to have this structure. Moreover, only Fe with the right structure and found at the surface can be an active site for the ORR. Catalyst FC280 is found right on the solid line (Figure 9A). This was expected because FC280 is synthesized in the same way as the catalysts represented by the squares. For the six other NNMCs of the present study, increased Fe content resulted in decreased activity.

An explanation of the descending part of the bell-shaped curve in Figure 9A was given in ref 78. Excess Fe can catalyze  $\text{NH}_3$  decomposition into  $\text{N}_2$  and  $\text{H}_2$ . Hydrogen is less reactive than  $\text{NH}_3$ , and consequently both the microporous area and N content decreased with increasing Fe content, resulting in a negative effect of excess Fe on the activity (78). For the present NNMC catalysts, that explanation cannot hold because heat treatment was done under an inert atmosphere (except FC280, M786, and DAL900C). Among the presently investigated catalysts (except FC280 and M786), no C support is used in the synthesis and the morphology of the catalyst depends on the carbonization–graphitization process of precursor molecules. One possible explanation to account for the descending part of Figure 9A is the catalysis of graphitization of the C precursor molecules by iron or iron carbide at 800–1000 °C. A higher graphitization would most probably be detrimental to the ORR activity of the resulting catalysts. Iron carbide is believed to be the catalyst responsible for carbon nanotube formation at temperatures of 700–1000 °C (121–123) or graphitization of C at temperatures <800 °C (124). This explanation goes well along with the peculiar behavior of catalysts UK63 and UK65 in Figure 9A: the micropore surface area and activity of these catalysts is high in spite of 3 wt % Fe because the excess Fe cannot form  $\text{Fe}_3\text{C}$  because of the presence of S in these catalysts (84), with Fe forming  $\text{Fe}_{1-x}\text{S}$  preferentially to iron carbide (91).

The N content of the catalysts is now scrutinized. Figure 9B shows that the total surface content in N does not determine the activity of the present NNMC or that of the previous data (squares). A similar cloud of points is obtained if the N content is restricted to pyridinic or pyrrolic N atoms. This means that, even though N atoms are known to be present in the active sites, the number of available N atoms is, in general, well in excess compared to other factors restricting the density of the active sites.

Next, the microporous surface area of the various NNMCs is looked at. Figure 10 shows that, despite some scattering, the data obtained on the present NNMC (black circles) show a trend of increasing activity with increased micropore surface area. By comparison with the trend observed previously (squares (77)), there seems, on the one hand, that a mismatch arises between the two groups of data. With the model especially developed for disordered carbonaceous materials (112–115) that does not show the artifacts engendered by the slit pore model at pore sizes of 8–9 and 22 Å (Figure 4 in ref 77), it is possible to investigate in even greater detail what exact pore sizes are important.

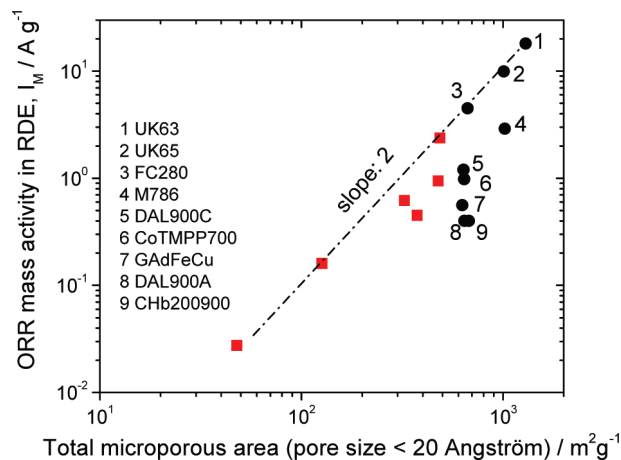


FIGURE 10. Mass activity in RDE vs microporous surface area of NNMCs. The red squares are literature data (reanalyzed with the present NLDFT model for the micropore surface) obtained on catalysts made by impregnation of the same amount of Fe on the same non-microporous C and heat treatment at 950 °C in  $\text{NH}_3$  for times of 2–62 min (77).

The total microporous surface area was subdivided into three areas defined by pore sizes (i) <5 Å, (ii) 5–7.5 Å, and (iii) 7.5–20 Å. The recurrent feedback of plots of activity versus different pore size intervals helped us to choose the above meaningful subdivisions. Figure 11 shows the relationship between the activity measured in RDE and each of these surface areas found in the catalysts. Quadrant A in Figure 11 shows two separate branches, one each for catalysts made with a preexisting C support (red squares and data point 3) and for catalysts made without a preexisting C support (all black circles, except points 3 and 4). Interestingly, point 4 found between the two trends corresponds to catalyst M786, which is made from a 50/50 wt % mix of a C support and of organic molecules. Quadrants B and C show a single branch for all data. The only data apart from the trend are those of UK63 and UK65 (points 1 and 2) in quadrant C. Quadrant D confirms for the present NNMCs that the mesoporous surface area (20–100 Å) does not correlate with the activity.

In conclusion, analysis of the isotherms with the model from Ustinov confirms the importance of micropores for NNMC synthesized in any of the ways described in the Experimental Methods section. The pores hosting active sites seem to be 5–20 Å wide. This is a more refined analysis compared to size <20 Å previously proposed (77). Possibly pores <5 Å may host a few active sites too, but their accessibility to  $\text{O}_2$  or  $\text{H}^+$  is very low for NNMCs synthesized without a preexisting C support, explaining the trend of the black circles in Figure 11A. The minimum pore size envisaged to host  $\text{FeN}_4$  active sites is the projected length of two Fe–N bonds at a 45° angle, 2.77 Å [ $1.96 \text{ Å} \cos(\pi/4)$ ]. If one, alternatively two, benzene rings (width 2.46 Å) are added on either side of the  $\text{FeN}_4$  central moiety, the width of the active site is 7.7 and 12.6 Å, respectively. The latter corresponds to the site structure envisaged by Figure 15 in ref 89.

Last, the slope in quadrants B and C (Figure 11) is about 2 in a log–log plane, meaning that the activity is proportional

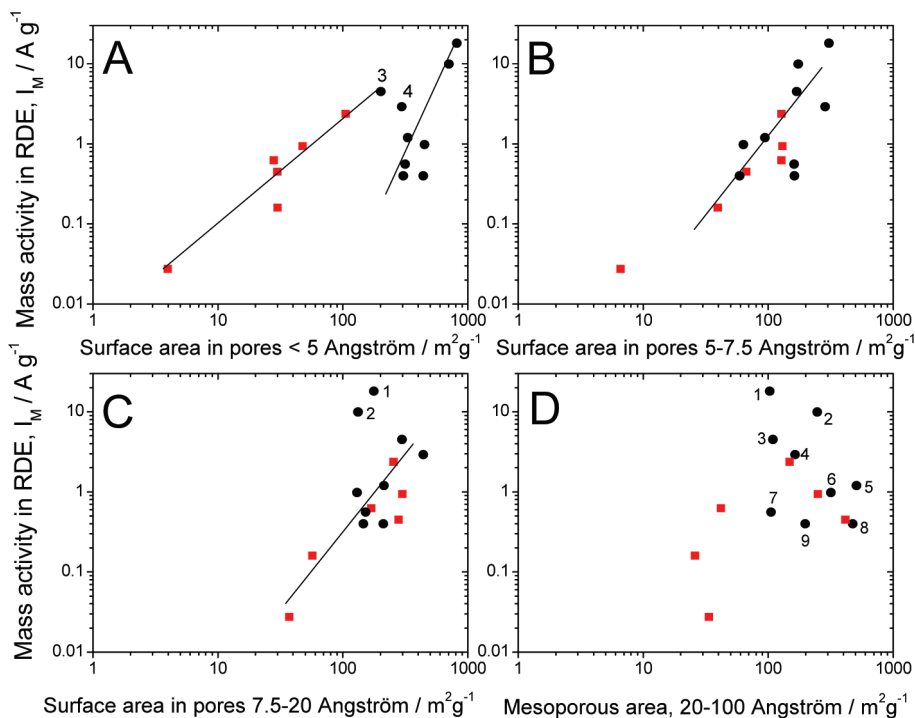


FIGURE 11. Mass activity in RDE vs surface area comprised of pores of specific sizes. The numbers correspond to the legend of Figure 10. The red squares are literature data (reanalyzed with the present NLDFT model for the micropore surface) obtained on catalysts made by impregnation of the same amount of Fe on the same non-microporous C and heat treatment at 950 °C in NH<sub>3</sub> for times of 2–62 min (77).

to the square of the surface areas defined by pores of 5–7.5 and 7.5–20 Å, respectively. No explanation for that fact can be proposed at this time.

**IX.3. Comparison of PEMFC vs RDE Mass Activities at 0.8 V.** For the second effect (ii) introduced in section IV, the improvement factor when changing from the RDE system to the PEMFC system might be represented by the ratio

$$[I_M(\text{PEMFC})/I_M(\text{RDE})]/[C_M(\text{PEMFC})/C_M(\text{RDE})] \quad (\text{VI})$$

where  $C_M$  is the mass capacitance. The division by the factor  $C_M(\text{PEMFC})/C_M(\text{RDE})$  is to take into account the sometimes observed change in  $C_M$  from the RDE system to the PEMFC system.

If the improvement factors (Figure 12) are solely due to the temperature activation of each single site, then we can estimate the values of activation energies,  $E_a$ , that would explain such improvements.  $E_a$  of 10, 20, 40, and 50 kJ mol<sup>-1</sup> would result in improvement factors from 20 to 80 °C of 2, 4, 16, and 32, respectively. Zhang et al. reported an improvement of the ORR activity of a factor 2 from 20 to 70 °C ( $E_a = 10$  kJ mol<sup>-1</sup>) for a non-heat-treated iron porphyrin in 0.5 M H<sub>2</sub>SO<sub>4</sub> (47). For Pt/C, Neyerlin et al. also found  $E_a = 10$  kJ mol<sup>-1</sup> (Table III in ref 120). Song et al. reported an improvement of the ORR activity by a factor of 7 from 20 to 70 °C ( $E_a = 35$  kJ mol<sup>-1</sup>) for a non-heat-treated cobalt phthalocyanine at pH 6 (49). On the other hand, non-heat-treated iron phthalocyanines showed decreased activity with increased temperature from 20 to 80 °C in 0.1 M H<sub>2</sub>SO<sub>4</sub> (125). From measurements on two catalysts, like FC280 and

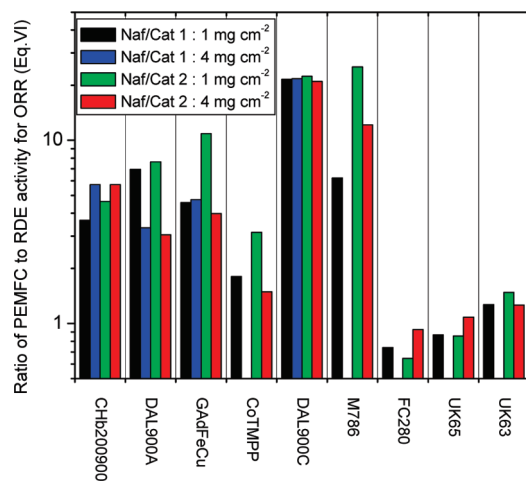


FIGURE 12. ORR mass activity normalized by mass capacitance: effect of a switch from the RDE system (20 °C) to the PEMFC system (80 °C).

M786 of the present study, we find an improvement factor of only 2–3 in RDE when the temperature is increased from 20 to 60 °C.

New studies to gain knowledge on  $E_a$  of NNMCs are important. Also, the optimization of the RDE ink formulation might reveal itself as important as the optimization of the PEMFC ink formulation in order to measure the true activity of such catalysts.

**IX.4. Perspectives for Making More Active NNMC.** Compared to Pt/C, the fundamentals for the ORR mass activity of NNMCs obtained from the heat treatment of Fe (Co), N, and C are less understood. This stems (i) from the incompletely resolved structure of the active sites of heat-treated NNMCs and (ii) from the incomplete knowledge of

the characteristics limiting their site density. The latter has impeded the practical efforts to improve the activity of such NNMCs. The present paper shows that micropores seem to be important for any NNMCs obtained from the heat treatment of metal (Fe and Co), N, and C.

This section reviews the information gathered mainly during the last 5 years on NNMCs obtained at INRS by the impregnation of iron acetate on carbon black followed by heat treatment in  $\text{NH}_3$ . The most recent views on what factors limit the activity of “impregnation NNMC” are then exerted on heat-treated NNMCs obtained from alternative synthesis schemes that were investigated in the present study.

The most accurate information on the structure of the active sites has been up to now obtained from EXAFS, which shows that Fe is coordinated by four N atoms. However, the remaining part of the site is important too because many non-heat-treated  $\text{Fe-N}_4$  chelates do not show a high activity, such as that observed with heat-treated NNMCs. Because the NNMC active sites are widely accepted to comprise Fe (Co), N, and C coordinated together in a particular way, all three may control the site density. Quite early, it was demonstrated for impregnated NNMCs that increasing the Fe content increased the activity up to a content of 0.2–0.5 wt %, beyond which the activity leveled off or decreased (63). The leveling off of the activity with Fe content  $>0.5$  wt % remained unexplained until recently (78). So, a piece of the puzzle was lacking. On the side of the C specific area, many different carbon powders with a wide range of specific areas were tested but neither the Brunauer–Emmett–Teller area or the resulting NNMCs correlated with the activity (126). Some high-surface-area C supports resulted in poorly active catalysts. Why? A new piece of the puzzle came into place when a connection was made between the amount of disordered C present in carbon black, the weight loss during pyrolysis in  $\text{NH}_3$ , and the N content after pyrolysis in  $\text{NH}_3$  (76). It was understood that the presence of disordered C in the initial C support is a paramount requirement to obtain a good activity after pyrolysis in  $\text{NH}_3$ . Disordered C reacts faster with  $\text{NH}_3$  than graphitic C, fixes the N from  $\text{NH}_3$  in the NNMC, serves as a highly transformable C source to build the active sites with, and moreover, its gasification by  $\text{NH}_3$  creates micropores *during* pyrolysis. When using non-microporous carbon blacks, micropore creation during pyrolysis in  $\text{NH}_3$  seems to be a requirement to obtain high activity (77, 89, 127, 128). The maximization of the micropore area requires minute control of the duration of pyrolysis, temperature of pyrolysis, and gas flow. In a next step, we started to work again on carbon blacks having a high microporous area before pyrolysis but having concomitantly a low content of disordered C. The most recent study on impregnation catalysts shows that the ORR activity obtained with as-received microporous carbon blacks is lower than that obtained with as-received non-microporous carbon blacks because what steers the ORR

activity is the micropore area created *during* pyrolysis, not its absolute value (129).

Interestingly, disordered C can also be deliberately introduced in the micropores of a high-surface-area C in the form of molecules. This is the approach that was adopted in the synthesis of M786. Black pearls was mixed with PTCDA in a 1:1 mass ratio. In order to be sure that the PTCDA molecules went into the micropores, the ball-milling technique was used. This catalyst yields the best activity of this study in PEMFC (Figure 3).

Now, our focus moves from “impregnation NNMC” to “bulk NNMC”. We call “bulk NNMC” catalysts those that are obtained without a preexisting C support. This implies that the Fe and C precursors can be homogeneously mixed in contrast to “impregnation NNMC”. Thus, in bulk NNMCs, Fe can be found at the surface but also in the bulk. Bulk NNMCs could potentially lead to a high density of active sites. However, one possible drawback is that a large proportion of the active sites may not be found at the surface. Such sites will not participate in the ORR. Incomplete Fe utilization is evidenced for one such particular catalyst by Figure 4 in ref 84. Another drawback of bulk NNMC is the lack of control on the organization of the precursor molecules into a partially graphitized carbonaceous material.

To alleviate the problems inherent to the “bulk NNMC” approach, several actions are possible. One is to avoid large agglomerates and low surface area by adding a foaming agent. Another is to ballmill bulk NNMC after pyrolysis. A third possible action is to create or to extend the porous network of bulk NNMC by subjecting it to a second heat treatment under a reactive atmosphere (84, 85, 88). The increase in the activity due to the second heat treatment can be of a decade. The exact conditions of the second heat treatment (temperature, time, and etching gas) need to be controlled precisely in order to connect the maximum number of active sites with the porous network extended during the second pyrolysis.

In summary, the focus during the preparation of NNMC from heat treatment should be on the control and optimization of the heat-treatment conditions, not so much on the chemicals used to start from. It is seen in the present paper that highly active NNMCs can be obtained from almost any source of Fe, N, and C. Thus, the proper conditions of heat treatment must be found for the various raw materials. The time of heat treatment has a paramount importance, especially in a reactive atmosphere such as  $\text{NH}_3$ ,  $\text{O}_2$ , or  $\text{CO}_2$ . Also, while up to now, NNMC synthesis has consisted of usually a single heat treatment followed by leaching of excess metal, reaching even more active NNMC will probably require several synthesis steps that may include two or more heat treatments (80, 81, 83–85, 88, 130), one or two ball-milling steps (88, 131) and acid washing. These multisteps must be performed in an appropriate sequence in order to achieve the highest possible site density.

## X. CONCLUSIONS

The mass activity for the ORR of the present NNMC is governed mainly by the surface area of micropores having a pore size of 5–20 Å (Figures 10 and 11) and might, as a secondary factor, be limited by their N content (Figure 9). The activity is not limited by the metal content (Figure 9).

The mass activity for the ORR of the present NNMC in a RDE spans from 0.4 to 18 A g<sup>-1</sup> at 0.8 V vs RHE and at 20 °C (Figure 1B), and that in PEMFC spans from 0.7 to 80 A g<sup>-1</sup> at 0.8 V vs RHE and at 80 °C (Figure 3). The ORR mass activity of the present NNMC is usually higher in the fuel cell than in RDE, up to a multiplication factor >20 (Figure 12). The reason for this huge difference is unresolved. Pt-based catalysts do not show such an effect. To explain this difference with such NNMCs, new comprehensive studies are needed on (i) the effect of the temperature on the mass activity of NNMC and on (ii) the optimization of the catalyst ink with respect to the Nafion ionomer and catalyst ratio for a correct measurement of the mass activity both in a RDE and a fuel cell.

Remaining tasks in the field of NNMCs are (i) further increasing the activity of such catalysts, (ii) improving the electrode fabrication and mass-transport properties, and (iii) developing a fundamental understanding of the factors affecting their stability or instability. The first task should be facilitated by the conclusions of this work and by the fact that some catalysts in the present work were found to be very active. The third task, not dealt with in this work, is now becoming the most important as the activity reaches acceptable values.

**Acknowledgment.** INRS acknowledges the support of NSERC and General Motors of Canada. E.A.U. acknowledges the Russian Foundation for Basic Research (Project 06-03-32268-a).

**Supporting Information Available:** Calculation of the volumetric activity for a Pt/C catalyst, full description of the catalyst's synthesis, summary of the RDE results with other ink recipes, definition of the target mass activity for NNMCs in RDE, discussion on the nature of the redox peaks seen in the N<sub>2</sub>-CV, and SEM pictures of all NNMCs. This material is available free of charge via the Internet at <http://pubs.acs.org>.

## REFERENCES AND NOTES

- Banerjee, S.; Curtin, D. E. *J. Fluorine Chem.* **2004**, *125*, 1211.
- Markovic, N. The hydrogen electrode reaction and the electrooxidation of CO and H<sub>2</sub>/CO mixtures on well-characterized Pt and Pt-bimetallic surfaces. In *Handbook of fuel cells—Fundamentals, technology and applications*; Vielstich, W.; Gasteiger, H. A., Lamm, A., Eds.; John Wiley and Sons: Chichester, U.K., 2003; Vol. 2; p 368.
- Jasinski, R. *Nature* **1964**, *201*, 1212.
- Markovic, N. M.; Gasteiger, H. A.; Ross, P. N. *J. Phys. Chem.* **1996**, *100*, 6715.
- Yang, Y. F.; Zhou, Y. H.; Cha, C. S. *Electrochim. Acta* **1995**, *40*, 2579.
- Lee, H. K.; Shim, J. P.; Shim, M. J.; Kim, S. W.; Lee, J. S. *Mater. Chem. Phys.* **1996**, *45*, 238.
- Meng, H.; Shen, P. K. *Electrochem. Commun.* **2006**, *8*, 588.
- Blizanac, B. B.; Ross, P. N.; Markovic, N. M. *Electrochim. Acta* **2007**, *52*, 2264.
- Demarconnay, L.; Coutanceau, C.; Léger, J. M. *Electrochim. Acta* **2004**, *49*, 4513.
- Rashkova, V.; Kitova, S.; Konstantinov, I.; Vitanov, T. *Electrochim. Acta* **2002**, *47*, 1555.
- Matsuki, K.; Kamada, H. *Electrochim. Acta* **1986**, *31*, 13.
- Roche, I.; Châinet, E.; Chatenet, M.; Vondrak, J. *J. Phys. Chem. C* **2007**, *111*, 1434.
- Gasteiger, H. A.; Kocha, S. S.; Sompalli, B.; Wagner, F. T. *Appl. Catal., B* **2005**, *56*, 9.
- U.S. Department of Energy, Multi-Year Research, Development and Demonstration plan: Planned Program Activities for 2005–2015 (2007), [http://www1.eere.energy.gov/hydrogenandfuelcells/mypp/pdfs/fuel\\_cells.pdf](http://www1.eere.energy.gov/hydrogenandfuelcells/mypp/pdfs/fuel_cells.pdf). Section 3.4, p 24.
- Mukerjee, S.; Srinivasan, S. *J. Electroanal. Chem.* **1993**, *357*, 201.
- Mukerjee, S.; Srinivasan, S.; Soriaga, M. P.; McBreen, J. J. *Electrochem. Soc.* **1995**, *142*, 1409.
- Mukerjee, S.; Srinivasan, S.; Soriaga, M. P.; McBreen, J. J. *Phys. Chem.* **1995**, *99*, 4577.
- Toda, T.; Igarashi, H.; Uchida, H.; Watanabe, M. *J. Electrochem. Soc.* **1999**, *146*, 3750.
- Min, M.; Cho, J.; Cho, K.; Kim, H. *Electrochim. Acta* **2000**, *45*, 4211.
- Thompson, D. Pt alloys as oxygen reduction catalysts. In *Handbook of fuel cells—Fundamentals, technology and applications*; Vielstich, W., Gasteiger, H. A., Lamm, A., Eds.; John Wiley and Sons: Chichester, U.K., 2003; Vol. 3; p 467.
- Ticianelli, E. A.; Derouin, C. R.; Redondo, A.; Srinivasan, S. *J. Electrochem. Soc.* **1988**, *135*, 2209.
- Wilson, M. S.; Gottesfeld, S. *J. Appl. Electrochem.* **1992**, *22*, 1.
- Wilson, M. S.; Gottesfeld, S. *J. Electrochem. Soc.* **1992**, *139*, L28.
- Zhang, J.; Lima, F. H. B.; Shao, M. H.; Sasaki, K.; Wang, J. X.; Hanson, J.; Adzic, R. R. *J. Phys. Chem. B* **2005**, *109*, 22701.
- Zhang, J.; Vukmirovic, M. B.; Sasaki, K.; Uribe, F.; Adzic, R. R. *J. Serb. Chem. Soc.* **2005**, *70*, 513.
- Vukmirovic, M. B.; Zhang, J.; Sasaki, K.; Nilekar, A. U.; Uribe, F.; Mavrikakis, M.; Adzic, R. R. *Electrochim. Acta* **2007**, *52*, 2257.
- Larminie, J.; Dicks, A. L. *Fuel Cell Systems Explained*, 2nd ed.; John Wiley and Sons Inc.: Hoboken, NJ, 2003.
- Gasteiger, H. A.; Panels, J. E.; Yan, S. G. *J. Power Sources* **2004**, *127*, 162.
- Dodelet, J. P. Oxygen reduction in PEM fuel cell conditions: heat-treated non-precious metal—N<sub>4</sub> macrocycles and beyond. In *N<sub>4</sub>-Macrocyclic Metal Complexes*; Zagal, J. H., Bedioui, F., Dodelet, J. P., Eds.; Springer Science + Business Media Inc.: New York, 2006; p 83.
- Organisation internationale des constructeurs automobiles, <http://oica.net/category/production-statistics>, 2007.
- Platinum 2008; Johnson Matthey: Hertfordshire, England, 2008; p 60; <http://www.platinum.matthey.com/publications/pgmreview.html>.
- <http://www.platinum.matthey.com>, 2008.
- Cawthorn, R. G. *South. Afr. J. Sci.* **1999**, *95*, 481.
- Jaffray, C.; Hards, G. Precious metal supply requirements. In *Handbook of fuel cells—Fundamentals, technology and applications*; Vielstich, W., Gasteiger, H. A., Lamm, A., Eds.; John Wiley and Sons: Chichester, U.K., 2003; Vol. 3; p 509.
- Pattabi, M.; Castellanos, R. H.; Castillo, R.; Ocampo, A. L.; Moreira, J.; Sebastian, P. J.; McClure, J. C.; Mathew, X. *Int. J. Hydrogen Energy* **2001**, *26*, 171.
- Susac, D.; Sode, A.; Zhu, L.; Wong, P. C.; Teo, M.; Bizzotto, D.; Mitchell, K. A. R.; Parsons, R. R.; Campbell, S. A. *J. Phys. Chem. B* **2006**, *110*, 10762.
- Feng, Y.; He, T.; Alonso-Vante, N. *Chem. Mater.* **2008**, *20*, 26.
- Lee, K.; Zhang, L.; Zhang, J. *Electrochem. Commun.* **2007**, *9*, 1704.
- Zhong, H.; Zhang, H.; Liu, G.; Liang, Y.; Hu, J.; Yi, B. *Electrochem. Commun.* **2006**, *8*, 707.
- Zhong, H.; Zhang, H.; Liang, Y.; Zhang, J.; Wang, M.; Wang, X. *J. Power Sources* **2007**, *164*, 572.
- Liu, G.; Zhang, H. M.; Wang, M. R.; Zhong, H. X.; Chen, J. *J. Power Sources* **2007**, *172*, 503.
- Ohnishi, R.; Takahashi, Y.; Takagaki, A.; Kubota, J.; Domen, K. *Chem. Lett.* **2008**, *37*, 838.

- (43) Jahnke, H.; Schönborn, M.; Zimmermann, G. *Top. Curr. Chem.* **1976**, *61*, 133.
- (44) Boulatov, R. Billion-year-old oxygen cathode that actually works: Respiratory oxygen reduction and its biomimetic analogs. In *N<sub>2</sub> Macrocyclic Metal Complexes*; Zagal, H., Bedioui, F., Dodelet, J. P., Eds.; Springer Science + Business Media: New York, 2006; p 1.
- (45) Song, E.; Shi, C.; Anson, F. C. *Langmuir* **1998**, *14*, 4315.
- (46) Shi, C.; Anson, F. C. *Inorg. Chem.* **1998**, *37*, 4294.
- (47) Zhang, L.; Song, C.; Zhang, J.; Wang, H.; Wilkinson, D. P. *J. Electrochem. Soc.* **2005**, A2421.
- (48) Baranton, S.; Coutanceau, C.; Roux, C.; Hahn, F.; Leger, J. M. *J. Electroanal. Chem.* **2005**, *577*, 223.
- (49) Song, C.; Zhang, L.; Zhang, J.; Wilkinson, D. P.; Baker, R. *Fuel Cells* **2007**, *7*, 9.
- (50) Bagotzky, V. S.; Tarasevich, M. R.; Radyushkina, K. A.; Levina, O. E.; Andrusyova, S. I. *J. Power Sources* **1977**, *2*, 233.
- (51) van Veen, J. A. R.; van Baar, J. F.; Kroese, K. J. *J. Chem. Soc., Faraday Trans.* **1981**, *1*, 2827.
- (52) Scherson, D. A.; Gupta, S. L.; Fierro, C.; Yeager, E. B.; Kordesch, M. E.; Eldridge, J.; Hoffman, R. W.; Blue, J. *Electrochim. Acta* **1983**, *28*, 1205.
- (53) Scherson, D.; Tanaka, A.; Gupta, S. L.; Tryk, D.; Fierro, C.; Holze, R.; Yeager, E. B. *Electrochim. Acta* **1986**, *31*, 1247.
- (54) Van der Putten, A.; Elzing, A.; Visscher, W.; Barendrecht, E. *J. Electroanal. Chem.* **1986**, *205*, 233.
- (55) Wiesener, K. *Electrochim. Acta* **1986**, *31*, 1073.
- (56) Tarasevich, M. R.; Radyushkina, K. A. *Mater. Chem. Phys.* **1989**, *22*, 477.
- (57) Franke, R.; Ohms, D.; Wiesener, K. *J. Electroanal. Chem.* **1989**, *260*, 63.
- (58) Yeager, E. B. *Electrochim. Acta* **1984**, *29*, 1527.
- (59) van Veen, J. A. R.; Colijn, H. A.; van Baar, J. F. *Electrochim. Acta* **1988**, *33*, 801.
- (60) Wiesener, K.; Ohms, D.; Neumann, V.; Franke, R. *Mater. Chem. Phys.* **1989**, *22*, 457.
- (61) Gupta, S. L.; Tryk, D.; Bae, I.; Aldred, W.; Yeager, E. B. *J. Appl. Electrochem.* **1989**, *19*, 19.
- (62) Côté, R.; Lalande, G.; Guay, D.; Dodelet, J. P.; Denes, G. *J. Electrochem. Soc.* **1998**, *145*, 2411.
- (63) Wang, H.; Côté, R.; Faubert, G.; Guay, D.; Dodelet, J. P. *J. Phys. Chem. B* **1999**, *103*, 2042.
- (64) Biloul, A.; Coowar, F.; Contamin, O.; Scarbeck, G.; Savy, M.; van den Ham, D.; Riga, J.; Verbist, J. *J. Electroanal. Chem.* **1990**, *289*, 189.
- (65) Fabjan, C.; Frithum, G.; Hartl, H. *Ber. Bunsenges. Phys. Chem.* **1990**, *94*, 937.
- (66) Ohms, D.; Herzog, S.; Franke, R.; Neumann, V.; Wiesener, K.; Gamburgcev, S.; Kaisheva, A.; Iliev, I. *J. Power Sources* **1992**, *38*, 327.
- (67) Bouwkamp-Wijnoltz, A. L.; Visscher, W.; van Veen, J. A. R.; Tang, S. C. *Electrochim. Acta* **1999**, *45*, 379.
- (68) Gojkovic, S. L.; Gupta, S.; Savinell, R. F. *J. Electroanal. Chem.* **1999**, *462*, 63.
- (69) Contamin, O.; Debiemme-chouvy, C.; Savy, M.; Scarbeck, G. *J. New Mater. Electrochem. Syst.* **2000**, *3*, 67.
- (70) Sun, G. Q.; Wang, J. T.; Gupta, S.; Savinell, R. F. *J. Appl. Electrochem.* **2001**, *31*, 1025.
- (71) Bogdanoff, P.; Herrmann, I.; Hilgendorff, M.; Dorbandt, I.; Fiechter, S.; Tributsch, H. *J. New Mater. Electrochem. Syst.* **2004**, *7*, 85.
- (72) Ye, S.; Vijn, A. K. *J. Solid State Electrochem.* **2005**, *9*, 146.
- (73) Herrmann, I.; Bogdanoff, P.; Schmithals, G.; Fiechter, S. *Electrochem. Soc. Trans.* **2006**, *3*, 211.
- (74) Medard, C.; Lefèvre, M.; Jaouen, F.; Dodelet, J. P.; Lindbergh, G. *Electrochim. Acta* **2006**, *51*, 3202.
- (75) Subramanian, N. P.; Kumaraguru, S. P.; Colon-Mercado, H.; Kim, H.; Popov, B. N.; Black, T.; Chen, D. A. *J. Power Sources* **2006**, *157*, 56.
- (76) Jaouen, F.; Charretier, F.; Dodelet, J. P. *J. Electrochem. Soc.* **2006**, *153*, A689.
- (77) Jaouen, F.; Lefèvre, M.; Dodelet, J. P.; Cai, M. *J. Phys. Chem. B* **2006**, *110*, 5553.
- (78) Jaouen, F.; Dodelet, J. P. *Electrochim. Acta* **2007**, *52*, 5975.
- (79) Maruyama, J.; Abe, I. *Chem. Commun.* **2007**, *27*, 2879.
- (80) Maruyama, J.; Abe, I. *J. Electrochem. Soc.* **2007**, *154*, B297.
- (81) Maruyama, J.; Okamura, J.; Miyazaki, K.; Abe, I. *J. Phys. Chem. C* **2007**, *111*, 6597.
- (82) Wang, P.; Ma, Z.; Zhao, Z.; Jia, L. *J. Electroanal. Chem.* **2007**, *611*, 87.
- (83) Maruyama, J.; Okamura, J.; Miyazaki, K.; Uchimoto, Y.; Abe, I. *J. Phys. Chem. C* **2008**, *112*, 2784.
- (84) Koslowski, U. I.; Abs-Wurmbach, I.; Fiechter, S.; Bogdanoff, P. *J. Phys. Chem. C* **2008**, *112*, 15356.
- (85) Koslowski, U. I.; Herrmann, I.; Bogdanoff, P.; Barkschat, C.; Fiechter, S.; Iwata, N.; Takahashi, H.; Nishikoro, H. *Electrochem. Soc. Trans.* **2008**, *13*, 125.
- (86) Sirk, A. H. C.; Campbell, S. A.; Birss, V. I. *J. Electrochem. Soc.* **2008**, *155*, B592.
- (87) Garsuch, A.; d'Eon, R.; Dahn, T.; Klepel, O.; Garsuch, R. R.; Dahn, J. R. *J. Electrochem. Soc.* **2008**, *155*, B236.
- (88) Wood, T. E.; Tan, Z.; Schmoekel, A. K.; O'Neill, D.; Atanasoski, R. *J. Power Sources* **2008**, *178*, 510.
- (89) Charretier, F.; Jaouen, F.; Ruggeri, S.; Dodelet, J. P. *Electrochim. Acta* **2008**, *53*, 2925.
- (90) Charretier, F.; Ruggeri, S.; Jaouen, F.; Dodelet, J. P. *Electrochim. Acta* **2008**, *53*, 6881.
- (91) Herrmann, I.; Koslowski, U. I.; Radnik, J.; Fiechter, S.; Bogdanoff, P. *Electrochem. Soc. Trans.* **2008**, *13*, 143.
- (92) Olson, T. S.; Chapman, K.; Atanassov, P. *J. Power Sources* **2008**, *183*, 557.
- (93) Pylypenko, S.; Mukerjee, S.; Olson, T. S.; Atanassov, P. *Electrochim. Acta* **2008**, *53*, 7875.
- (94) Artyushkova, K.; Levendosky, S.; Atanassov, P.; Fulghum, J. *Top. Catal.* **2007**, *46*, 263.
- (95) Artyushkova, K.; Pylypenko, S.; Olson, T. S.; Fulghum, J. E.; Atanassov, P. *Langmuir* **2008**, *24*, 9082.
- (96) Ziegelbauer, J. M.; Olson, T. S.; Pylypenko, S.; Alamgir, F.; Jaye, C.; Atanassov, P.; Mukerjee, S. *J. Phys. Chem. C* **2008**, *112*, 8839.
- (97) Garsuch, A.; McIntyre, K.; Michaud, X.; Stevens, D. A.; Dahn, J. R. *J. Electrochem. Soc.* **2008**, *155*, B953.
- (98) Garsuch, A.; Sattler, R. R.; Witt, S.; Klepel, O. *Microporous Mesoporous Mater.* **2006**, *89*, 164.
- (99) Bard, A. J.; Faulkner, L. R. *Electrochemical Methods: Fundamentals and Applications*; John Wiley & Sons: New York, 1980.
- (100) Jimenez-Mateos, J. M.; Fierro, J. L. G. *Surf. Interface Anal.* **1996**, *24*, 223.
- (101) Casanovas, J.; Ricart, J. M.; Rubio, J.; Illas, F.; Jimenez-Mateos, J. M. *J. Am. Chem. Soc.* **1996**, *118*, 8071.
- (102) Faubert, G.; Côté, R.; Dodelet, J. P.; Lefèvre, M.; Bertrand, P. *Electrochim. Acta* **1999**, *44*, 2589.
- (103) Karweik, D. H.; Winograd, N. *Inorg. Chem.* **1976**, *15*, 2336.
- (104) Roe, S. P.; Hill, J. O.; Magee, R. J. *Augst. J. Chem.* **1986**, *39*, 1377.
- (105) Tarazona, P. *Phys. Rev. A* **1985**, *31*, 2672.
- (106) Tarazona, P.; Marconi, U. M. B.; Evans, R. *Mol. Phys.* **1987**, *60*, 573.
- (107) Seaton, N. A.; Walton, J. P. R. B.; Quirke, N. *Carbon* **1989**, *27*, 853.
- (108) Lastoskie, C.; Gubbins, K. T.; Quirke, N. *J. Phys. Chem.* **1993**, *97*, 4786.
- (109) Ravikovitch, P. I.; Neimark, A. V. *Stud. Surf. Sci. Catal.* **2000**, *129*, 597.
- (110) Tikhonov, A. N.; Arsenin, V. Y. *Solutions of ill-posed problems*; Wiley: New York, 1977.
- (111) Gardner, L.; Kruk, M.; Jaroniec, M. *J. Phys. Chem. B* **2001**, *105*, 12516.
- (112) Ustinov, E. A.; Do, D. D.; Fenelonov, V. B. *Carbon* **2006**, *44*, 653.
- (113) Ustinov, E. A.; Do, D. D.; Jaroniec, M. *Appl. Surf. Sci.* **2005**, *252*, 548.
- (114) Ustinov, E. A.; Do, D. D.; Fenelonov, V. B. *Appl. Surf. Sci.* **2007**, *253*, 5610.
- (115) Ustinov, E. A.; Kukushkina, J.; Sokolov, V.; Kravchik, A.; Tereshchenko, G.; Melgunov, M.; Eletski, P.; Yakovlev, V.; Fenelonov, V. A refined method of porous structure analysis of activated carbons with N<sub>2</sub> adsorption isotherms. International Conference on Carbon (CARBON'08), Nagano, Japan, 2008.
- (116) Bonakdarpour, A.; Lefevre, M.; Yang, R.; Jaouen, F.; Dahn, T.; Dodelet, J. P.; Dahn, J. R. *Electrochem. Solid-State Lett.* **2008**, *11*, B105.
- (117) Bonakdarpour, A.; Delacote, C.; Yang, R.; Wieckowski, A.; Dahn, J. R. *Electrochem. Commun.* **2008**, *10*, 611.
- (118) Lowell, S. *Introduction to powder surface area*; John Wiley & Sons: New York, 1979.



- (119) Herrmann, I. In *Innovative Elektrokatalyse: Platinfreie Kathodenkatalysatoren für Brennstoffzellen*; Vdm Verlag: Saarbrücken, 2008; p 153.
- (120) Neyerlin, K. C.; Gu, W.; Jorne, J.; Gasteiger, H. A. *J. Electrochem. Soc.* **2006**, *153*, A1955.
- (121) Hou, H.; Schaper, A. K.; Weller, F.; Greiner, A. *Chem. Mater.* **2002**, *14*, 3990.
- (122) Perez-Cabero, M.; Rodriguez-Ramos, I.; Guerrero-Ruiz, A. *J. Catal.* **2003**, *215*, 305.
- (123) Schaper, A. K.; Hou, H.; Greiner, A.; Phillipp, F. *J. Catal.* **2004**, *222*, 250.
- (124) Sinclair, R.; Itoh, T.; Chin, R. *Microsc. Microanal.* **2002**, *8*, 288.
- (125) Baker, R.; Wilkinson, D. P.; Zhang, J. *Electrochim. Acta* **2008**, *53*, 6906.
- (126) Jaouen, F.; Marcotte, S.; Dodelet, J. P.; Lindbergh, G. *J. Phys. Chem. B* **2003**, *107*, 1376.
- (127) Jaouen, F.; Dodelet, J. P. *J. Phys. Chem. C* **2007**, *111*, 5963.
- (128) Jaouen, F.; Serventi, A. M.; Lefevre, M.; Dodelet, J. P.; Bertrand, P. *J. Phys. Chem. C* **2007**, *111*, 5971.
- (129) Lefevre, M.; Dodelet, J. P. *Electrochim. Acta* **2008**, *53*, 8269.
- (130) Herranz, J.; Lefevre, M.; Larouche, N.; Stansfield, B.; Dodelet, J. P. *J. Phys. Chem. C* **2007**, *111*, 19033.
- (131) Proietti, E.; Ruggeri, S.; Dodelet, J. P. *J. Electrochem. Soc.* **2008**, *155*, B340.

AM900219G